Metal Halide Perovskite Nanocrystal Solar Cells: Progress and Challenges

Chongming Liu, Qingsen Zeng, Haotong Wei, Yue Yu, Yue Zhao, Tanglue Feng, and Bai Yang*

Perovskite nanocrystal (PNC) solar cells have attracted increasing interest in recent years because of their excellent optoelectronic properties and unique advantages, which distinguish them from conventional nanocrystals and their bulk counterparts. This emerging type of photovoltaic is promising but faces many challenges regarding commercialization. Therefore, a comprehensive review is presented on the recent progress and current challenges in PNC solar cells. It begins by reviewing the optoelectronic, unique properties of PNCs for photovoltaic devices. Then, the limiting factors on performance are detailed and analyzed with respect to the Shockley–Queisser limit, followed by a summary of effective strategies for efficiency improvement alongside other promising ideas. Finally, the present challenges are discussed toward high-efficiency, stable, easy-to-process, and low-cost, commercial, PNC photovoltaics. This review aims to attract further attention to the design and development of PNC solar cells, which will accelerate their progress.

1. Introduction

In the last decade, metal halide perovskite materials with the chemical formula ABX_3, where A, B, and X are usually monovalent cations ($CH_3NH_3^+$ or MA^+, $HC(NH_2)_2^+$ or FA^+, Cs^+), divalent metal cations (Pb^{2+}, Sn^{2+}), and halide ions (Cl^-, Br^-, I^-), respectively, have attracted significant attention due to their outstanding properties, including: a high absorption coefficient,[1–4] narrow bandwidth emission,[5,6] low trap state density,[7–11] long carrier diffusion length and lifetimes,[9,12–14] and high carrier mobility.[13,15] These competitive advantages have triggered wide applications in various photoelectronic devices.[16] However, unlike with bulk perovskite materials, perovskite nanocrystals (PNCs) did not become independent of mesoporous materials and suitable for further applications until 2014, when the first nontemplate synthesis of PNCs was reported by Schmidt et al.,[17] although PNCs were discovered in single crystals in 1999.[18] Subsequently, PNCs with different chemical compositions were synthesized by various methods, including hot-injection methods,[19] ligand-assisted reprecipitation,[20,21]

ultrasonication methods,[22] solvothermal approaches,[23] microwave-assisted synthesis,[24] and mechanical grinding.[25] PNCs not only inherit perovskite properties, but also possess the features of nanomaterials, such as their size-confinement effect and ease of processing as a colloidal ink, making PNCs suitable for incorporation into various electronic devices and compatible with printing techniques.[19,26] Moreover, nanoscale perovskites exhibit superior phase stability, particularly for $CsPbI_3$ and $FAPbI_3$, due to their lattice construction and large surface energy.[27,28] Compared with traditional II–VI and III–V semiconductor nanocrystals, PNCs also exhibit unique properties.[29–32] Firstly, facile synthesis with inexpensive precursors can be conducted at room temperature with PNCs without inert gas protection. PNCs also have a bandgap ranging from the ultraviolet to near-infrared, through which they can be easily tuned by size management and composition adjustment. Furthermore, they exhibit narrow bandwidth emission (<100 meV) over the entire visible range. PNCs also exhibit a fluorescence quantum yield near unity without additional passivation due to the defect-tolerance effect. Finally, they also demonstrate negligible self-absorption and Förster resonance energy transfer. These remarkable characteristics make PNCs more favorable than their bulk counterparts and traditional semiconductor nanocrystals. Thus, PNCs have promising applications in light-emitting diodes (LEDs),[33] lasers,[34] photodetectors,[35,36] and solar cells.[28]

In 2016, Luther et al. first used $CsPbI_3$ PNCs to fabricate solar cells using a layer-by-layer approach.[28] The solar cell exhibited an extremely high open-circuit voltage (V_{OC}) of 1.23 V, which was ≈85% of the Shockley–Queisser (S–Q) limited V_{OC}, and a high power conversion efficiency (PCE) of 10.77%. This value was comparable to those of state-of-the-art PbS nanocrystal solar cells,[37] indicating the potential of PNC solar cells. To date, the highest PCE achieved by PNC solar cells has reached 17.39%.[38] Though PCEs have shown rapid, significant improvements, they are still limited compared to solar cells fabricated by bulk perovskite materials. Moreover, most studies on PNC solar cells have only been reported over the past two years. Research on PNC solar cells is still in its infancy, leaving substantial room for further improvement.

Herein, we review the progress in the field of PNC solar cells. This review starts with detailing the unique advantages of PNCs. Next, we analyze current factors limiting their performance and

C. Liu, Dr. Q. Zeng, Prof. H. Wei, Y. Yu, Dr. Y. Zhao, T. Feng, Prof. B. Yang
State Key Laboratory of Supramolecular Structure and Materials
College of Chemistry
Jilin University
Changchun 130012, P. R. China
E-mail: byangchem@jlu.edu.cn

The ORCID identification number(s) for the author(s) of this article can be found under https://doi.org/10.1002/smtd.202000419.

**ADVANCED
SCIENCE NEWS**
www.advancedsciencenews.com

**small
methods**
www.small-methods.com

summarize the corresponding effective strategies for systematically improving their performance, with respect to the S–Q limit. Finally, we emphasize the challenges and deficiencies impeding further development. This review provides a comprehensive understanding of PNC solar cells and an updated overview of recent results in order to inspire further development.

2. Unique PNC Properties

As an emerging material for use as a solar cell absorber, the performance of PNC devices still lags behind its bulk counterparts, which have achieved PCE values of 25.2%.[39] However, this should not overshadow the excellent properties of PNCs. Instead of their general properties, which have been introduced in detail by other reviews, in this section we focus on the unique properties and advantages of PNCs for photovoltaic applications, including their excellent processability, defect-tolerance, potential to surpass the Shockley–Queisser limit, and intrinsic, low, open-circuit voltage loss.

2.1. Excellent Processability

Generally, conventional perovskite solar cell films are deposited through either a one or two-step spin coating method using the precursor solution, sometimes with an extra antisolvent dropping, followed by an annealing procedure to further promote grain growth.[40,41] Film formation is complicated by crystal nucleation and growth processes during the film deposition process.[42] Thus, to ensure the high reproducibility and quality of the final film, precise control of the deposition conditions is necessary, including the precursor solution temperature,[42] solvent ratio of the precursor solution,[43] and annealing temperature.[44] PNCs obtain high crystallinity during synthesis and are subsequently deposited through a layer-by-layer method, leading to a highly reproducibility.[45] The use of crystalline PNCs also neglects the impact of substrate effects on crystallization.[46] Furthermore, the solubility limit of Br in the precursor solution (0.4–0.43 M in N,N-dimethylformamide (DMF)) is not a challenge for PNCs.[47,48] The flexible composition adjustment ensures that PNCs with various compositions can

be synthesized[49] Particularly, for FA-mixed type perovskites, PNCs exhibit more compositional tunability than that of their bulk phase counterparts.[46,50] Moreover, the synthesis and film deposition procedures for PNCs avoid the use of strong polar solvents, such as DMF and dimethyl sulfoxide (DMSO), with no need for subsequent annealing procedures.[28,51] Given that their excellent solubility in nonpolar solvents makes them compatible with various film fabrication techniques, such as spray-coating, printing, and roll-to-roll processing, PNCs are promising for future, large-scale solar cell production.[26,52]

2.2. Defect Tolerance

Despite the low concentration of defects in traditional semiconductors (parts per million or parts per billion), they still have a serious impact on the conductivity, free carrier mobility, and carrier lifetime of semiconductors.[53] Hence, an excellent photovoltaic device requires a high electronic quality with an ultralow defect concentration. However, PNCs have a high defect concentration due to their large surface-to-volume ratio and low formation energy.[54–56] Despite this, PNCs exhibit a high photoluminescence quantum yield (PLQY) without surface passivation, unlike traditional semiconductor nanocrystals.[57] This anomalous phenomenon results from a high tolerance to defects, denoted the defect tolerance effect. Several calculations with different models have indicated multiple factors are responsible for this effect.[55,56,58,59]

The electronic structure of $APbX_3$ perovskite is special. The valence band maximum (VBM) is determined by the halide 3/4/5p and Pb 6s atomic orbitals and the conduction band minimum (CBM) is mainly dominated by the Pb 6p atomic orbital.[30] The bandgap is formed between two antibonding orbitals. The electronic structure is distinct from that of a conventional semiconductor, where the valence band (VB) is composed of bonding states.[30] For this unique electronic structure, the vacancies only slightly affect the electronic structure and act as shallow traps or deep localized states hybridized with the conduction band (CB) and VB, both of which do not capture charges (**Figure 1**a). The most harmful deep traps are antisites and interstitials located inside the bandgap, which result in a loss in charge collection efficiency due to induced recombination.[56,58]
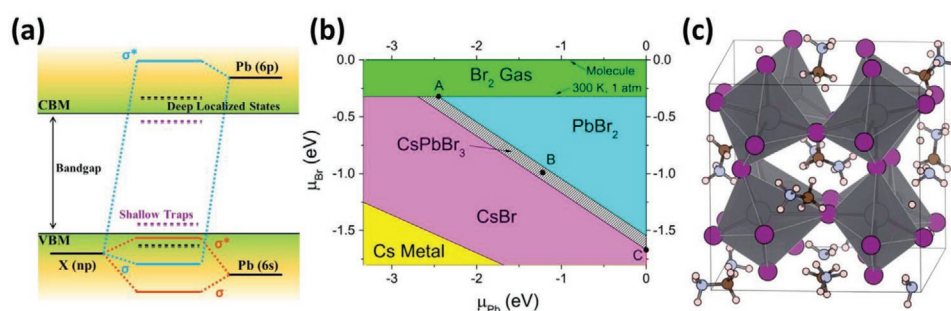

Figure 1. a) Schematic representation of the electronic structure of defect tolerant PNCs. σ and σ^* correspond to the bonding and antibonding orbitals. b) Stability regions of different compounds against Br and Pb chemical potentials. The shaded region indicates the available equilibrium chemical potential region for CsPbBr₃. Three representative points A (Pb-poor condition), B (moderate condition), and C (Pb-rich condition) were chosen to calculate the defect formation energy (Table 1). Reproduced with permission.[55] Copyright 2017, American Chemical Society. c) A snapshot from a molecular dynamics simulation showing the structure of MAPbI₃ perovskite. Reproduced with permission.[62] Copyright 2015, American Chemical Society.

**ADVANCED
SCIENCE NEWS**
www.advancedsciencenews.com

**small
methods**
www.small-methods.com

Table 1. Calculated formation energies (in eV) for defects in CsPbBr$_3$ at the three chosen points A, B, and C in Figure 1b.

	Cs$_{Br}$	Cs$_i$	Pb$_i$	Pb$_{Br}$	Pb$_{Cs}$	V$_{Br}$	Br$_{Cs}$	Br$_{Pb}$	Cs$_{Pb}$	Br$_i$	V$_{Cs}$	V$_{Pb}$
A	6.22	3.55	4.66	6.28	2.44	2.67	0.80	1.40	0.81	0.70	0.20	0.49
B	4.77	2.77	3.44	4.38	1.99	2.00	2.25	3.30	1.26	1.37	0.98	1.71
C	3.27	1.95	2.22	2.48	1.59	1.32	3.75	5.20	1.66	2.05	1.80	2.93

Note: Vacancies (V$_{Cs}$, V$_{Pb}$, V$_{Br}$); Interstitials (Cs$_i$, Pb$_i$, Br$_i$); Antisites (Cs$_{Pb}$, Cs$_{Br}$, Pb$_{Br}$, Pb$_{Cs}$, Br$_{Cs}$, Br$_{Pb}$).

Nevertheless, there is typically a low concentration of interstitials and antisites due to their high formation energy. Only vacancies with relatively low formation energies are typically observed. As shown in Figure 1b and **Table 1**, for CsPbBr$_3$, vacancies on the A or X sites are always the domain defects under different conditions.[55] In short, the formation of harmful defects in perovskite is severely constrained.

Additionally, the deformation of the soft [PbX$_3$]$^-$ sublattice coupled with a carrier can form a large polaron, whose screened coulomb potential reduces charge carrier scattering with defects and longitudinal, optical phonons.[30,60,61]

Finally, the type of A-site cation is not the decisive factor in achieving defect tolerance, as the electronic structure is mainly determined by the orbitals of Pb and the halide; however, the cation modulates the electronic properties.[58,60] The reorientational motions of the organic cation within the [PbX$_3$]$^-$ cage, as shown in Figure 1c, accelerate polaron formation and protect the carrier more rapidly. The polaron formation time of CsPbBr$_3$ (0.7 ps) is more than double the time of MAPbBr$_3$ (0.3 ps).[60,62] In addition, the introduction of an organic cation enlarges the material dielectric constant. A high dielectric constant is beneficial for protecting the carriers from grain boundary scattering and charged defects. Thus, perovskites with organic cations could improve the defect tolerance effect.[58]

2.3. Potential to Surpass the Shockley–Queisser Limit

2.3.1. Slow Relaxation of Hot Carriers

The absorption of photons with energy greater than the bandgap energy creates hot carriers, which have excess kinetic energy above the band edges. Immediately after photoexcitation, hot carriers relax to the band edge through ultrafast scattering with carriers or phonons, leading to carrier thermalization and subsequent carrier cooling to achieve thermal equilibrium with the lattice (**Figure 2**a).[63,64] If hot carriers are used before thermalization, a PCE of up to 66% (AM 1.5 illumination, 300 K) can be achieved theoretically, breaking the S–Q limit for single junction solar cells.[65]

Even so, it is difficult to harvest hot carriers for conventional semiconductors due to their ultrafast relaxation process, on the femtosecond (fs) time scale, resulting from the Coulomb potential.[61] However, ABX$_3$ perovskite exhibits a slow relaxation process caused by large polaron formation,[66] a hot-phonon bottleneck,[67] and Auger heating effects.[64] Zhu et al. reported a long hot carrier lifetime > 100 picosecond (ps) in MAPbBr$_3$ and FAPbBr$_3$.[66] An unexpectedly long hot carrier lifetime in FASnI$_3$ was recorded up to a few nanoseconds (ns).[68] The remarkably long carrier lifetime in perovskite ensures a long transport distance. In MAPbI$_3$, the quasiballistic transport length for initial hot carriers was reported as 230 nm, which was significantly longer than that of GaAs (85 nm),[69] Si (20 nm),[70] and GaN (14 nm).[71] Furthermore, a 600 nm transport limit could be achieved before thermal equilibrium.[72] Surprisingly, quantum confinement of PNCs is beneficial to further increase the hot carrier lifetime of perovskite.[73] Li et al. systematically studied the hot carrier relaxation mechanism in MAPbBr$_3$ PNCs, bulk MAPbBr$_3$, and traditional NCs. At both low and high carrier densities, PNC hot carriers exhibited higher temperature and longer lifetimes (Figure 2b). They found that confined PNCs exhibited suppressed Auger recombination, an enhanced intrinsic bottleneck effect (weak energy dispersion of longitudinal optical phonons, which hindered their interaction with acoustic phonons) at low carrier densities, and an extra Auger heating effect at high carrier densities, compared to traditional NCs. With decreasing crystal size, the longitudinal, optical phonon decay time increased, indicating that carrier relaxation induced by phonons was dramatically hindered (Figure 2c). Finally, they achieved ≈83% hot carrier extraction from the treated PNC film within 1 ps, compared to only ≈25% extraction in the bulk film.[73]

Although the excellent hot carrier properties of PNCs have exhibited tremendous potential for realizing high performance photovoltaic applications, the benefits of hot carriers in high performance solar cells have not been experimentally realized. The efficient utilization of hot carriers, as well as their theoretical study, is still an open question. In particular, the carrier-interface transfer requires more attention[74] and hot carrier extraction materials should be further exploited.[63]

2.3.2. Efficient Multiple Exciton Generation

When the excess kinetic energy of a hot carrier surpasses a certain threshold, the excess energy creates extra electron–hole (e–h) pairs with low energies via the Coulomb interaction, instead of converting into heat.[46,50] This process, called multiple exciton generation (MEG), reduces the carrier cooling loss and can increase the photovoltaic PCE to greater than 40%.[75–77] Utilization of the carrier multiplication effect is more practical than catching hot carriers, resulting in a reported external quantum efficiency (EQE) greater than 100% in lead chalcogenide, quantum dot-based solar cells.[78–80] Compared to bulk semiconductors, conventional, strong-quantum-confined NCs display enhanced Coulomb coupling and relaxed momentum conservation, which enhances the MEG process. However, their contribution to the photovoltaic PCE is still modest resulting
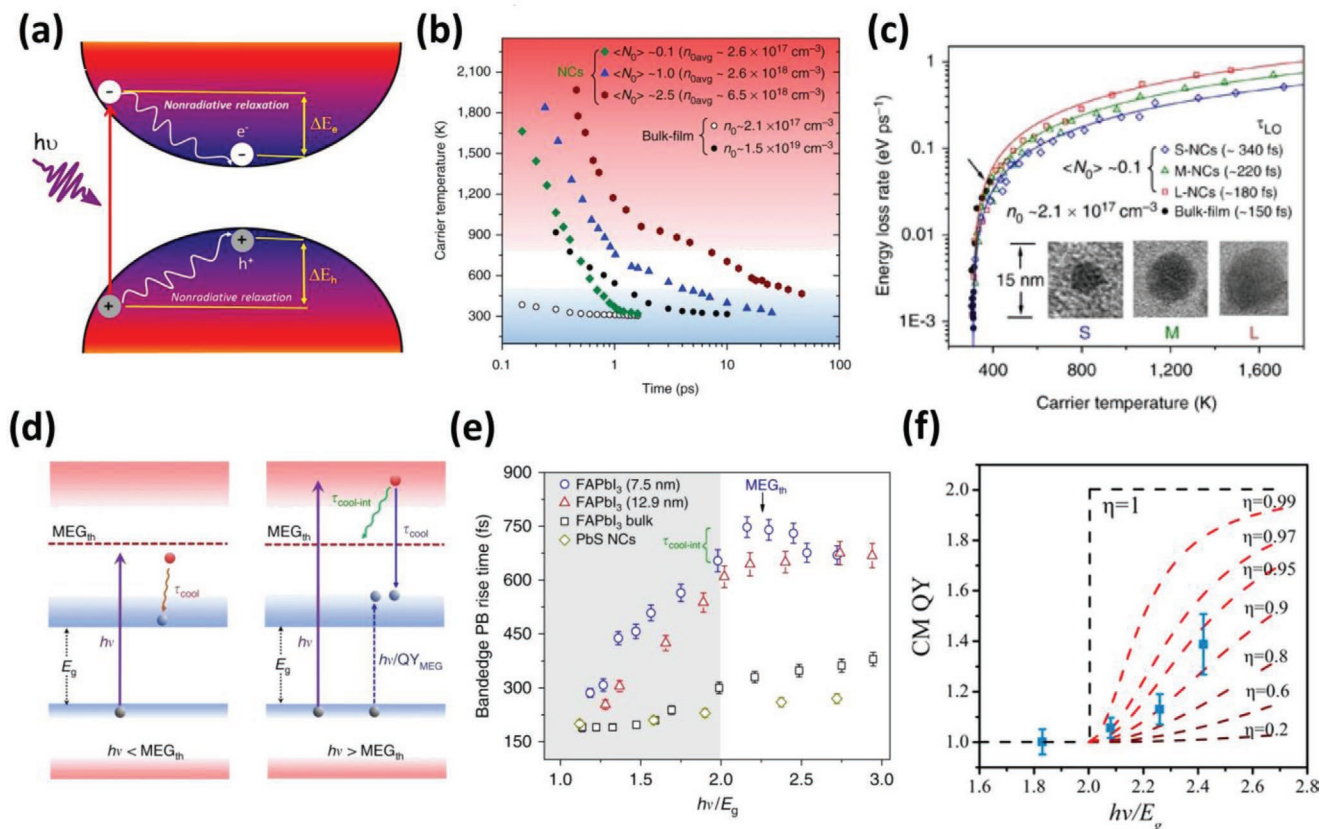
Figure 2. a) Schematic diagram representing hot carrier relaxation dynamics in the system. Reproduced with permission.[16] Copyright 2017, American Chemical Society. b) Hot carrier temperature as a function of delay time for MAPbBr$_3$ PNCs and bulk films with different carrier densities. c) Energy loss rate of hot carriers as a function of carrier temperature T_c for MAPbBr$_3$ PNCs and a MAPbBr$_3$ bulk film. Inset shows the representative TEM images of small (S), medium (M), and large (L) PNCs. Reproduced with permission.[73] Copyright 2017, Springer Nature. d) Schematic for hot carrier cooling (left) below the MEG threshold and (right) above the MEG threshold. $\tau_{cool\text{-}int}$ is the interval cooling time from the initial photoexcited state to the MEG threshold state. T_{cool} is the total cooling time of the hot carriers from various photoexcited states to the band-edge. e) Band-edge photobleaching buildup-time extracted from transient absorption spectroscopy of FAPbI$_3$ NCs with different sizes for polycrystalline bulk film and PbS NCs. Reproduced with permission.[75] Copyright 2018, Springer Nature. Gray region indicates the energies below the ideal MEG threshold of $2E_g$. f) Carrier multiplication quantum yield (CMQY) as a function of relative pump photon energy ($h\nu/E_g$) for CsPbI$_3$ NCs. Reproduced with permission.[46] Copyright 2020, American Chemical Society.

from the low MEG efficiency (η_{MEG}) and high MEG threshold energy ($E_{th} \approx 3E_g$).[46,75,81] The relationship between these variables is expressed as following[82,83]

$$E_{th} = E_g + \varepsilon_{ex} \quad (1)$$

$$\eta_{MEG} = \frac{E_g}{\varepsilon_{ex}} \quad (2)$$

$$\varepsilon_{ex} = \frac{h\nu - E_g}{QY - 1} \quad (3)$$

where ε_{ex} is the required excess energy for each e–h generation and E_g is the semiconductor bandgap. The ε_{ex} is determined by the exciton quantum yield (QY), which represents the number of e–h pairs excited by one photon with energy $h\nu > 2E_g$, where h is Planck's constant and ν is the photon frequency. To realize efficient MEG, a large QY for low ε_{ex} is necessary, requiring slow hot carrier relaxation according to the QY calculation[83]

$$QY = 1 + \prod_{i=1}^{n=1} \frac{k_{MEG}^i}{k_{MEG}^i + k_{relax}} + \prod_{i=1}^{n=2} \frac{k_{MEG}^i}{k_{MEG}^i + k_{relax}} + \cdots + \prod_{i=1}^{n=m} \frac{k_{MEG}^i}{k_{MEG}^i + k_{relax}} \quad (4)$$

ki_{MEG} is the rate of generation of $i+1$ e–h pairs from i hot excitons and k_{relax} is the carrier relaxation rate.

As discussed, in Section 2.3.1., PNCs exhibit excellent hot carrier properties, providing a long time window for MEG. Unsurprisingly, both Han et al. and Gregorkiewicz et al. observed a high η_{MEG} exceeding 90% with an E_{th} approaching $2E_g$ in CsPbI$_3$ PNCs.[46,50] However, remarkably, the nanocrystal size is critical for efficient MEG.[46] Based on FAPbI$_3$ PNCs, Li et al. proposed an inverse Auger process to illustrate the MEG mechanism, shown in Figure 2d. The total hot carrier relaxation was divided into two stages: an initial stage from the initial photoexcited state to the MEG threshold state; and subsequent stage from the MEG threshold state to the band edge. The relaxation time of the initial stage in small PNCs was much longer than in the subsequent stage (Figure 2e) and the MEG process was also enhanced due to the enhanced Coulomb coupling. However, small, conventional NCs with strong confinement led to

a reduced final density of states, which increased the E_{th}. Finally, they demonstrated an enhanced MEG ($\eta_{MEG} = 75\%$, $E_{th} = 2.25 E_g$) that surpassed that of conventional NCs.[75] Likewise, a recent study demonstrated the same result for $CsPbI_3$ PNCs but they ascribed the efficient MEG (Figure 2f, $\eta_{MEG} > 90\%$) to enhanced Coulomb coupling because the hot carrier relaxation time was similar in both the weak- and strong-confined $CsPbI_3$ PNCs.[46]

MEG in PNCs is a recently discovered phenomenon and more work should focus on the impacts of surface, ligands, constituents, and the shape of PNCs.[81] However, considering the success of lead chalcogenide, quantum dot-based solar cells, a large photovoltaic potential is likely and will be harnessed with further research.

2.4. Intrinsically Low Open-Circuit Voltage Losses

The open-circuit voltage losses of PNC solar cells are extremely low, especially when compared to their all-inorganic bulk counterparts. In 2016, the first PNC solar cell with a $CsPbI_3$ composition was created with a high V_{OC}, up to 1.23 V, which remains higher than current, bulk $CsPbI_3$ solar cells.[28] An ultrahigh V_{OC} of 1.28V with a V_{OC} loss of only 0.45 eV, the lowest for an inorganic, perovskite solar cell, was obtained via polymer-assisted passivation and charge extraction.[26] Using $CsPbBrI_2$ PNCs, Zeng et al. achieved a V_{OC} of 1.32 V with a V_{OC} loss of 0.5 eV.[48] The high V_{OC} values in PNC solar cells are not a coincidence. Luther et al. demonstrated that $Cs_XFA_{1-X}PbI_3$ PNC devices displayed increased V_{OC} values compared to their bulk counterparts.[84] We summarize the main device parameters of all reported PNC solar cells in **Table 2**. **Figure 3**a plots the V_{OC} versus the bandgap for different compositions and Figure 3b shows the voltage fraction (V_{OC}/V_{OC-SQ}), where V_{OC-SQ} is the theoretical, S–Q-limited V_{OC} of a single junction solar cell under a given bandgap.[85] Most I-rich, PNC solar cells demonstrate high fractions, particularly FA-containing cells. An increase bandgap results in an increased deviation from V_{OC-SQ}, because less e–h pairs are generated, inducing lower carrier densities in the bands and causing slight Fermi-level splitting.[85,86] Although, for Br-rich, PNC solar cells, relatively high V_{OC} values can be achieved due to the increased bandgap,[86] the V_{OC}/V_{OC-SQ} ratio is extremely low. Suri et al. studied the experimental impact of different alloys of PNCs on the V_{OC} and systematically analyzed how A-site and X-site substitution influenced the V_{OC} through time-resolved microwave conductivity (TRMC) measurements, as shown in Figure 3c. They concluded that the replacement of I^- with Br^- resulted in fast carrier recombination and poor charge transport, thus resulting in severe V_{OC} loss, but that the introduction of FA^+ mitigated the adverse effect.[49] Hazarika et al. also concluded that FA^+ controlled the V_{OC} loss[84] and it has been proven that the formation energies of deep traps become large in FA-containing PNCs.[87] These works are in accordance with our statistics.

Despite the PNC composition, I-rich, PNC solar cells indeed exhibit low V_{OC} losses. Liu et al. reviewed the energy loss in perovskite solar cells, where any undesirable, available electronic states, such as band tails or energy disorders and deep traps, caused V_{OC} loss.[86] Thus, low V_{OC} loss is related to perfect electronic states. Based on the same device architecture, Hao et al. compared the V_{OC} loss in a PNC solar cell and bulk

solar cell with the same composition of $Cs_{0.25}FA_{0.75}PbI_3$. They demonstrated that the PNC device exhibited a reduced, nonradiative, recombination-induced V_{OC} loss of 90 meV inside the film and 30 meV at the surface (Figure 3d). They conducted an investigation of light intensity-dependent V_{OC} losses to further study the recombination in the device (Figure 3e,f). At high light intensities, the PNC device was dominated by band-to-band recombination with an ideality factor of $n_{id} = 1$. However, in the bulk device, the n_{id} remained at 1.8, close to 2, indicating that the recombination was mainly trap-assisted,[87] It seems the PNC exhibited a stronger defect-tolerance. The synthesis of $CsPbX_3$ PNCs with excess Pb and the instability of oleylammonium halide surface species led to a Pb-rich surface.[54] Several theoretical and experimental studies have demonstrated that a Pb-rich condition leads to a low defect concentration.[55,56,88–91] While for $FAPbX_3$, synthesis with a FA-rich condition and DFT calculations indicated that deep traps were more difficult to generate in the presence of FA.[87]

Ultralow V_{OC} loss is distinct to PNC solar cells, particularly for I-rich components. Although this excellent property has been preliminary studied, deeper analysis should be conducted to clarify the origin of reduced V_{OC} losses and further control V_{OC} loss.

3. PNC Characterization

Alongside the synthesis methods and basic properties of PNCs, the normal characterization techniques for PNCs and solar cells have also been studied and reviewed by other works.[92–94] Thus, here we briefly introduce PNC characterization techniques with regards to defects, stability, and ligands, that are crucial for assessing the final device performance.

PNCs with high defect densities do not result in high device performance if no additional treatment is taken to passivate the defects.[95] PNCs with low defect densities always demonstrate a high photoluminescence (PL) intensity, slow decay of transient absorption (TA) or time-resolved photoluminescence (TRPL), high PLQY, and small Stokes shift (defined as the energy difference between the absorption and emission peaks).[7,95,96] To obtain further insight into the degree of electronic disorder of PNCs, the Urbach energy (E_U) can be extracted from the following equation[47,97]

$$\alpha = \alpha_0 \times \exp\left(\frac{E - E_0}{E_U}\right) \tag{5}$$

where α and E are the absorption coefficient and photon energy, respectively. Both α_0 and E_0 are material constants. A low Urbach energy represents superior photophysical properties.[95]

The stability of PNCs is fragile, which will be further discussed in Section 5.3. The agglomeration and phase transition can be directly observed by normal characterization techniques or even the naked eye during exterior changes or long-term storage.[7,96,98] However, it is necessary to deeply understand the instability through high-resolution characterization techniques to solve this problem. By combining in situ Raman spectroscopy and X-ray diffraction techniques, Li et al. studied the thermal stability of $CsPbX_3$ PNCs and found that both $CsPbI_3$ and $CsPbBr_3$ PNCs experienced a highly disordered state before

ADVANCED
SCIENCE NEWS

www.advancedsciencenews.com

small
methods

www.small-methods.com

Table 2. Device parameters of reported PNC solar cells.

	Device structure	Thickness [nm]	J_{SC} [mA cm^{-2}]	V_{OC} [V]	FF [%]	PCE [%]	SPO [%]	Max V_{OC} [V]	Band gap (eV)	V_{OC} Loss (eV)	Date	Ref.
1	FTO/TiO$_2$/CsPbI$_3$/Spiro/MoOx/Al	150	13.47	1.23	65	10.77	7.9	1.23	1.75	0.52	2016/10/6	[28]
2	FTO/TiO$_2$/CsPbI$_3$/Spiro/MoOx/Al/MgF$_2$	350	14.37	1.2	78	13.4		1.2	1.75	0.55	2017/10/27	[51]
3	FTO/TiO$_2$/CsPbI$_3$/PTAA/Au	300	13.59	1.18	72.6	11.64		1.18	1.73	0.55	2018/5/4	[111]
4	FTO/TiO$_2$/Mn-doped CsPbI$_3$/PTAA/Au	300	11.75	1.192	78.3	10.97	10.75	1.192	1.8	0.608	2018/5/7	[145]
5	FTO/TiO$_2$/CsPbI$_3$/Spiro/MoOx/Ag	400	12.24	1.06	73	9.47		1.06	1.74	0.68	2018/5/10	[162]
6	FTO/TiO$_2$/CsPbI$_3$/Spiro/MoO$_3$/Ag	200–300		1.2		12		1.2	1.75	0.55	2018/7/25	[106]
7	FTO/TiO$_2$/CsPbI$_3$/PTB7/MoO$_3$/Ag	300	12.39	1.27	80	12.55	12.35	1.28	1.73	0.45	2018/9/10	[26]
8	FTO/TiO$_2$/CsPbI$_3$/Spiro/MoOx/Al	300	15.5	1.18	73	13.47	12.37	1.18	1.74	0.56	2018/9/25	[84]
9	FTO/TiO$_2$/CsPbI$_3$/Spiro/Au	220	11.3	1.094	66	8.1		1.094	1.73	0.636	2018/12/10	[163]
10	FTO/TiO$_2$/CsPbI$_3$/Spiro/Au	220	14.8	1.11	74	12.15		1.11	1.86	0.75	2019/1/14	[126]
11	FTO/TiO$_2$/CsPbI$_3$/Spiro/Au	287	16.98	1.04	67.2	11.87	11	1.04	1.73	0.69	2019/4/10	[108]
12	FTO/TiO$_2$/CsPb$_{0.9}$Sb$_{0.1}$I$_3$/Spiro/Au	400	13.15	1.04	69	9.4				0	2019/5/22	[130]
13	FTO/TiO$_2$/CsPbI$_3$/PTAA/MoO$_3$/Ag	300	14.96	1.248	75.6	14.1	13.9	1.248	1.753	0.505	2019/6/23	[45]
14	ITO/TiO$_2$/CsPbI$_3$/Spiro/MoOx/Al	300	15.75	1.17	74	13.67	12.15	1.17	1.74	0.57	2019/6/28	[38]
15	FTO/TiO$_2$/CsPbI$_3$/Spiro/MoOx/Al	100–400	16.37	1.2	75	14.74		1.2	1.72	0.52	2019/7/16	[49]
16	FTO/TiO$_2$/Yb-doped CsPbI$_3$/PTB7/MoO$_3$/Ag	300	14.18	1.25	74	13.12		1.25	1.77	0.52	2019/8/10	[131]
17	FTO/TiO$_2$/CsPbI$_3$/Spiro/MoOx/Ag	300	15.21	1.18	74.2	13.3		1.23	1.76	0.53	2019/9/25	[107]
18	FTO/TiO$_2$/CsPbI$_3$/Spiro/Au		14.4	1.11	70	11.2	10.6	1.11	1.76	0.65	2019/9/26	[52]
19	FTO/TiO$_2$/CsPbI$_3$/PTAA/MoO$_3$/Ag	300–500	13.83	1.25	72	12.3		1.25	1.76	0.51	2019/10/1	[138]
20	ITO/SnO$_2$/CsPbI$_3$/Spiro/Au	350	15.4	1.16	53.9	9.6		1.21	1.76	0.55	2020/1/20	[87]
21	FTO/TiO$_2$/m-TiO$_2$/CsPbI$_3$/Spiro/Au	400	17.77	1.06	75.8	14.32	13.87	1.1	1.75	0.65	2020/1/22	[113]
22	FTO/TiO$_2$/CsPbI$_3$/PBDB-T:PNCs/PTAA/MoO$_3$/Ag	300	15.1	1.22	75	13.8		1.22	1.76	0.54	2020/4/1	[164]
23	ITO/TiO$_2$/CsPbBrI$_2$/P3HT/Au	200	13.13	1.3	70.4	12.02	9.5	1.32	1.82	0.5	2018/1/15	[48]
24	FTO/TiO$_2$/CsPbBrI$_2$/Spiro/Au	140	5.32	1.3	77	5.34		1.31	1.92	0.61	2018/3/19	[165]
25	FTO/TiO$_2$/CsPbBrI$_2$/Spiro/MoOx/Ag	400	11.72	0.97	62	7.04		0.97	1.92	0.95	2018/5/10	[162]
26	FTO/TiO$_2$/CsPbBr$_2$I/Spiro/MoOx/Ag	400	9.31	0.96	59	5.27		0.96	2.33	1.37	2018/5/10	[162]
27	FTO/TiO$_2$/CsPbBr$_{1.5}$I$_{1.5}$/Spiro/MoOx/Ag	400	11.35	1	70	7.94		1	2.19	1.19	2018/5/10	[162]
28	FTO/TiO$_2$/CsPbBr$_{0.24}$I$_{2.76}$/Spiro/MoOx/Al	100–400	14.99	1.13	60	10.39					2019/7/16	[49]
29	FTO/TiO$_2$/CsPbBr$_{0.36}$I$_{2.64}$/Spiro/MoOx/Al	100–400	11.61	1.14	62	8.19		1.16	1.79	0.63	2019/7/16	[49]
30	FTO/TiO$_2$/CsPbBr$_{0.39}$I$_{2.61}$/Spiro/MoOx/Al	100–400	10.36	1.08	47	5.32					2019/7/16	[49]
31	FTO/TiO$_2$/CsPbBr$_{2.1}$I$_{0.9}$/Spiro/MoOx/Al	100–400	6.3	1.16	53	3.87		1.24	2.03	0.79	2019/7/16	[49]
32	FTO/TiO$_2$/CsPbBr$_{2.85}$I$_{0.15}$/Spiro/MoOx/Al	100–400	2.36	1.39	59	1.92		1.39	2.25	0.86	2019/7/16	[49]
33	ITO/TiO$_2$/CsPbBrI$_2$/P3HT/Au	340	14.22	1.2	71.3	12.2		1.24	1.92	0.68	2020/3/18	[102]
34	ITO/TiO$_2$/CsPbBr$_3$/Spiro/Au	550	5.653	1.536	62.4	5.42		1.536	2.38	0.844	2016/12/22	[116]
35	ITO/TiO$_2$/mp-TiO$_2$/CsPbBr$_3$/Spiro/Au	800	8.55	0.859	0.57	4.21		0.859	2.4	1.541	2017/9/28	[166]
36	FTO/TiO$_2$/CsPbBr$_3$/Spiro/Au	350	7.01	1.42	53	5.6		1.4	2.3	0.9	2017/10/25	[167]
37	FTO/ZnO NPs/CsPbBr$_3$-CsPb$_2$Br$_5$/Spiro/Au	300	6.17	1.43	77.2	6.81	6.4	1.46	2.32	0.86	2018/2/1	[168]
38	FTO/TiO$_2$/CsPbBr$_3$/Spiro/MoOx/Ag	400	7.38	0.9	40	2.65		0.9	2.39	1.49	2018/5/10	[162]
39	FTO/TiO$_2$/CsPbBr$_3$/Spiro/Au	450	9.41	1.34	36	4.57		1.34	2.3	0.96	2020/1/8	[169]
40	ITO/SnO$_2$/FAPbI$_3$/Spiro/Au	150–200	11.83	1.1	64.42	8.38	8.05	1.1	1.55	0.45	2018/8/9	[27]
41	FTO/TiO$_2$/FAPbI$_3$/Spiro/MoOx/Al	300	11.81	1.12	64	8.52	8.83	1.12	1.55	0.43	2018/9/25	[84]
42	FTO/TiO$_2$/FAPbI$_3$/Spiro/MoOx/Al	100–400	13.61	1.09	80	11.96		1.12	1.55	0.43	2019/7/16	[49]
43	ITO/SnO$_2$/FAPbI$_3$/Spiro/Ag	200–300	15.4	1.1	74.8	12.7	12.7	1.1	1.65	0.55	2019/7/25	[105]
44	FTO/TiO$_2$/FAPbI$_3$/PTAA/MoO$_3$/Ag	300–400	15.97	1.15	66	12.01		1.15	1.52	0.37	2019/10/1	[138]
45	FTO/TiO$_2$/FAPbI$_3$/PBDB-T:PNCs/PTAA/MoO$_3$/Ag	300	16.7	1.12	71	13.2		1.12	1.52	0.4	2020/4/1	[164]

**ADVANCED
SCIENCE NEWS**

www.advancedsciencenews.com

**small
methods**

www.small-methods.com

Table 2. Continued.

|	Device structure	Thickness [nm]	J_{SC} [mA cm^{-2}]	V_{OC} [V]	FF [%]	PCE [%]	SPO [%]	Max V_{OC} [V]	Band gap (eV)	V_{OC} Loss (eV)	Date	Ref.
46	FTO/TiO$_2$/Cs$_{0.25}$FA$_{0.75}$PbI$_3$/Spiro/MoOx/Al	300	14.37	1.1	66	10.41	10.41	1.1	1.57	0.47	2018/9/25	[84]
47	FTO/TiO$_2$/Cs$_{0.5}$FA$_{0.5}$PbI$_3$/Spiro/MoOx/Al	300	14.8	1.13	62	10.42	10.26	1.13	1.63	0.5	2018/9/25	[84]
48	FTO/TiO$_2$/Cs$_{0.75}$FA$_{0.25}$PbI$_3$/Spiro/MoOx/Al	300	14.36	1.15	68	11.14	10.93	1.15	1.66	0.51	2018/9/25	[84]
49	ITO/TiO$_2$/Cs$_{0.25}$FA$_{0.75}$PbI$_3$/CsPbI$_3$/Spiro/ MoOx/Al	300	18.91	1.2	76	17.39	15.52	1.21	1.74	0.53	2019/6/28	[38]
50	ITO/TiO$_2$/Cs$_{0.25}$FA$_{0.75}$PbI$_3$/Spiro/MoOx/Al	300	14.99	1.15	66	11.43	6.49	1.15	1.58	0.43	2019/6/28	[38]
51	FTO/TiO$_2$/CsPbI$_3$/FAPbI$_3$/PTAA/MoO$_3$/Ag	700	17.26	1.22	74	15.6	15.1	1.22	1.76	0.54	2019/10/1	[138]
52	ITO/SnO$_2$/Cs$_{0.5}$FA$_{0.5}$PbI$_3$/Spiro/Au	350	18.3	1.17	78.3	16.6		1.17	1.64	0.47	2020/1/20	[87]
53	FTO/TiO$_2$/FAPbBr$_{0.48}$I$_{2.52}$/Spiro/MoOx/Al	100–400	15.21	1.14	65	11.43		1.14	1.61	0.47	2019/7/16	[49]
54	FTO/TiO$_2$/FAPbBr$_{1.26}$I$_{1.74}$/Spiro/MoOx/Al	100–400	11.09	1.19	62	8.21		1.19	1.8	0.61	2019/7/16	[49]
55	FTO/TiO$_2$/FA$_{0.81}$Cs$_{0.19}$PbBr$_{0.57}$I$_{2.43}$/Spiro/ MoOx/Al	100–400	12.86	1.18	63	9.59		1.18	1.64	0.46	2019/7/16	[49]
56	FTO/TiO$_2$/FA$_{0.55}$Cs$_{0.45}$PbBr$_{1.35}$I$_{1.65}$/Spiro/ MoOx/Al	100–400	11.07	1.24	60	8.23		1.27	1.82	0.55	2019/7/16	[49]
57	FTO/TiO$_2$/FA$_{0.26}$Cs$_{0.74}$PbBr$_{2.22}$I$_{0.78}$/Spiro/ MoOx/Al	100–400	10.4	1.2	49	6.13		1.29	2.03	0.74	2019/7/16	[49]
58	ITO/TiO$_2$/CsSnCl$_3$/Spiro/Au	150	19.82	0.87	56	9.66					2016/11/21	[133]
59	ITO/TiO$_2$/CsSnBr$_3$/Spiro/Au	150	21.23	0.85	58	10.46					2016/11/21	[133]
60	ITO/TiO$_2$/CsSnI$_3$/Spiro/Au	150	23.2	0.86	65	12.96					2016/11/21	[133]
61	ITO/PEDOT:PSS/CsSnI$_3$/PCBM/Ag	150				5.03	≈4.1				2019/2/18	[170]
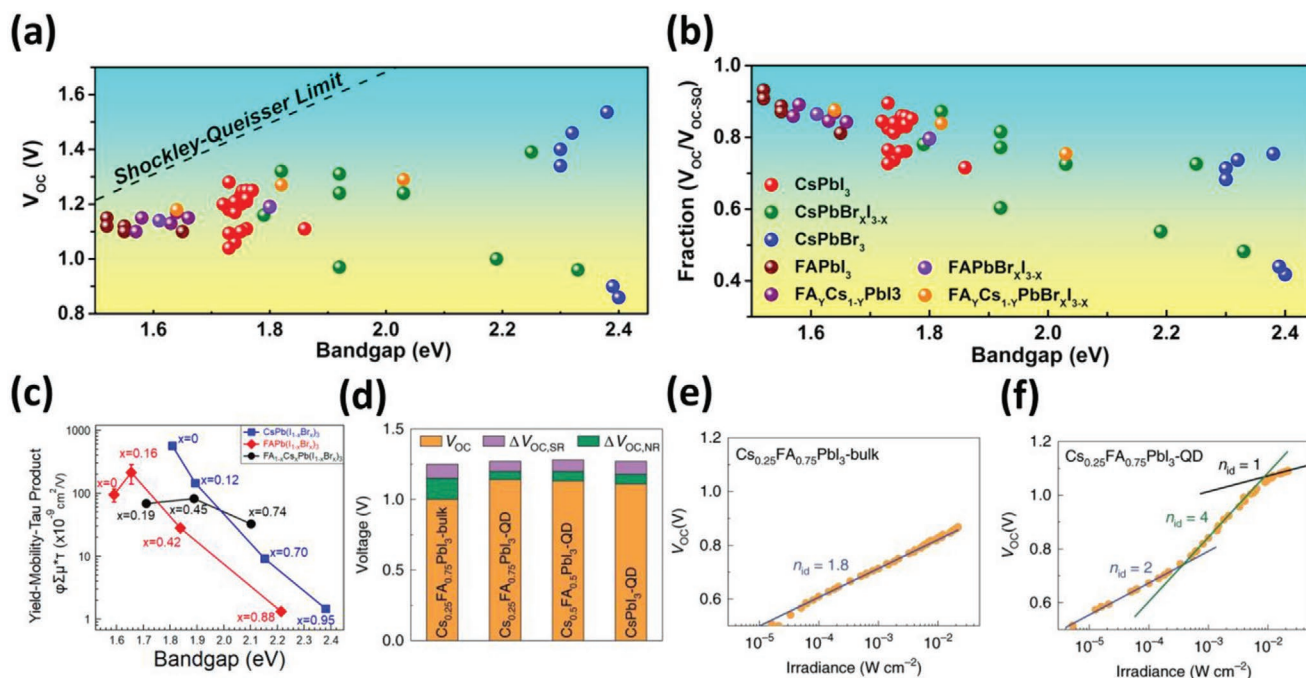
Figure 3. a) V_{OC} of PNC devices with various compositions versus their bandgaps. The dashed line represents the Shockley–Queisser limit for V_{OC}. b) The fraction of $V_{OC}/V_{OC\text{-}SQ}$ for PNC devices with various compositions versus their bandgaps. c) Yield–mobility–tau product determined by TRMC of various PNC films on quartz substrates. Reproduced with permission.[49] Copyright 2019, American Chemical Society. d) V_{OC} loss due to surface recombination (SR) and nonradiative recombination (NR) in bulk and PNC devices. Light intensity-dependent V_{OC} measurements over a large dynamic range in e) a Cs$_{0.25}$FA$_{0.75}$PbI$_3$-Bulk device and f) a Cs$_{0.25}$FA$_{0.75}$PbI$_3$-PNC device. Reproduced with permission.[87] Copyright 2020, Springer Nature.

decomposition.[99] Sun et al. conducted high-angle annular dark-field (HAADF) imaging experiments on CsPbI$_3$ PNCs through scanning transmission electron microscopy (STEM). They observed that, at the atomic scale, polar solvents induced lattice rotation and metal cation loss and revealed how stable CsPbI$_3$ PNC nanocubes evolved into nanowires.[98]

The ligands anchored on the PNC surface play an extremely important role in determining the PNC properties and final device performance, which we will discuss later in Section 4.2.1. Fourier-transform infrared spectroscopy (FTIR) and nuclear magnetic resonance (NMR) spectroscopy are effective characterization techniques for detecting ligand species.[100] When combined with other characterization techniques, NMR spectroscopy is the most functional. First, the interaction between the ligands and PNC surface can be confirmed or compared through the Stokes–Einstein equation[7,100]

$$D = \frac{k_B T}{6\pi\eta C} \tag{6}$$

where k_B, T, and η are the Boltzmann constant, absolute temperature, and solvent viscosity, respectively. The diffusion coefficient (D) can be obtained by diffusion ordered spectroscopy (DOSY), which is an NMR technique. On the molecular level, the capacity of the object (C) equals the solvodynamic radius. For cuboidal PNCs, $C = 0.66d$ where d is the cube length, which can be obtained by transmission electron microscopy (TEM). Variation in the diffusion constant between free ligands and anchored ligands on PNCs, and deviation between the calculated PNC size and the real size can be used to characterize the interaction between the ligands and PNCs.[7,100] The ligand density can also be calculated using a combination of the particle size measured by TEM, the concentration of ligands obtained by NMR spectroscopy, and the molar concentration of the PNCs detected by inductively coupled plasma (ICP) spectroscopy.[27,101] More conveniently, the mass fraction of the ligands can be obtained using the NMR internal standard method or a thermogravimetric (TG) measurement.[7,102]

4. Device Performance

4.1. Limitation of the Photovoltaic Performance of PNCs

As discussed, in Section 3, PNCs exhibit many unique properties for photovoltaic applications, particularly their potential to reach a high PCE. However, so far, it is unsatisfactory that the PCEs of PNC solar cells remain far below the S–Q limit. The highest recorded V_{OC} has reached >90% of V_{OC-SQ}; however, there is still room for improvement for the short-circuit current density (J_{SC}) (**Figure 4**a,b). Only three points exceed 80%
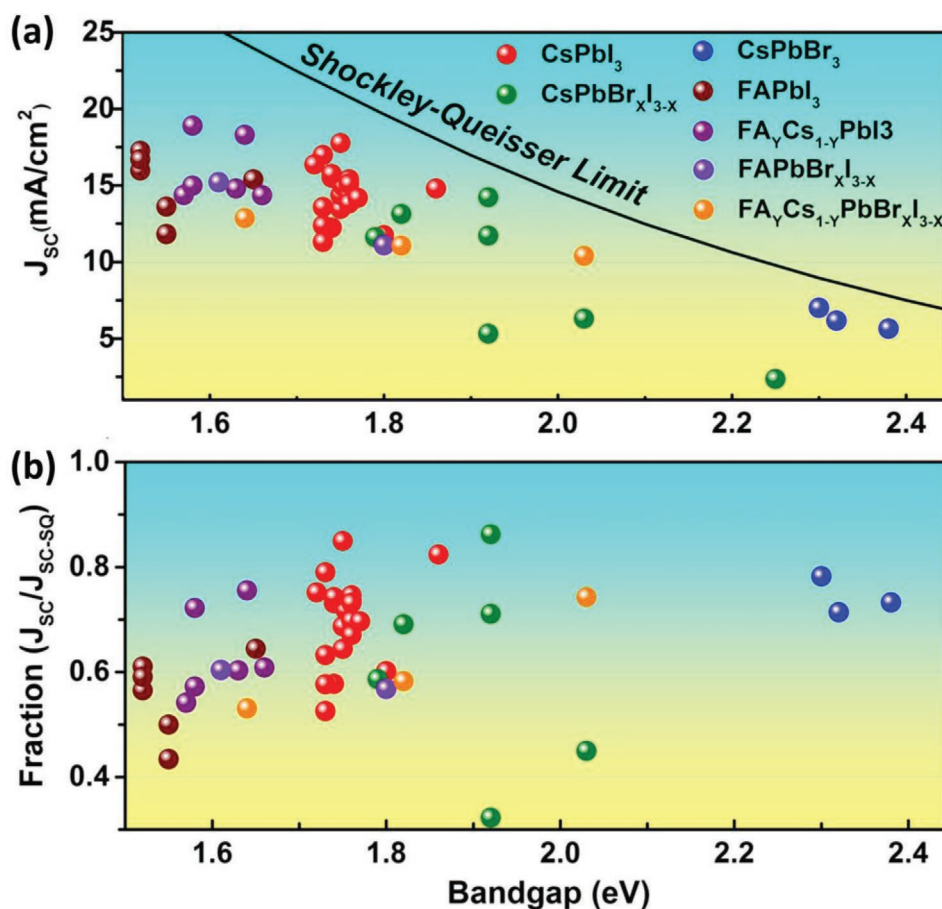

Figure 4. a) J_{SC} of PNC devices with various compositions versus their bandgaps. The dashed line represents the Shockley–Queisser limit for J_{SC}. b) The fraction of J_{SC}/J_{SC-SQ} of PNC devices with various compositions versus their bandgaps.

**ADVANCED
SCIENCE NEWS**
www.advancedsciencenews.com

**small
methods**
www.small-methods.com

of the S–Q limit with the highest fraction approximately 85%. PNC solar cells with narrow bandgaps possessed relatively high J_{SC} values but only reached 75% of the S–Q limit. Thus, to further increase the PCE, a higher J_{SC} must be achieved. Complete absorption of light is necessary for high J_{SC} values, which requires a film thickness of ≈5 µm.[103] Theoretical simulation of PNCs has demonstrated a large diffusion length (>9.2 µm) with a remarkably high carrier mobility (≈4500 cm^2 V^{-1} s^{-1}).[104] However, there is a large gap between simulation and reality. As shown in Table 2, the film thicknesses of PNC solar cells with excellent performances are ≈350 nm, which is insufficient for light absorption. Simply increasing the film thickness will decrease the carrier extraction efficiency because of the transport limitations in the PNC film and the significantly higher exciton binding energy compared to bulk materials, which will result in carrier loss through recombination.[31,51,105] Current limitations are mainly attributed to poor electronic coupling and complicated surface chemistry. Therefore, in terms of charge separation, transportation, and extraction, we summarize the current effective strategies for systematically improving device performance.

4.2. Progress of PNC Solar Cells

4.2.1. Surface Improvement

Ligand bonding to the surface of PNCs is a double-edged sword. On the one hand, ligands not only ensure good dispersibility and stability but also cover the defects.[28,45] Although perovskite PNCs are defect tolerant, they are not defect impervious.[7,54,95] On the other hand, long, insulating ligands trap charges inside the PNCs and increase the interparticle distance, resulting in poor electronic coupling.[27,45,51] In addition, the dielectric environment is closely correlated with the electronic coupling, influencing the total energy of a confined exciton.[45]

The film fabrication of current PNC solar cells is mostly based on a layer-by-layer method that was reported in the initial study on PNC solar cells (**Figure 5**a). In this method, the PNC film is swiftly dipped in Pb(OAc)$_2$ or Pb(NO$_3$)$_2$ saturated dimethyl acetate (MeOAc) then rinsed with neat MeOAc to partially remove the long chain ligands, which has been used as a moisture-dependent ligand exchange process in subsequent work.[28] In this ligand exchange process, long oleate ligands (OA) are exchanged with shorter acetate molecules, which are formed in situ via hydrolysis of MeOAc (Figure 5b). However, long oleylammonium ligands (OLA) still remain on the surface of the PNCs after this treatment.[106] Based on the first ligand exchange process, Sanehira et al. applied a FAI salt post-treatment (Figure 5a) to exchange the OLAs with FA (Figure 5b). They achieved an impressive carrier mobility boost from 0.23 to 0.50 cm^2 V^{-1} s^{-1} and a corresponding J_{SC} increase from 9.22 to 14.37 mA cm^{-2} with an antireflective MgF$_2$ coating.[51] However, the hydrolysis of MeOAc produced methanol, which led to the formation of metal hydroxide on the PNC surfaces, which served as trap states. Given this adverse effect, Kim et al. replaced the Pb-based ionic salts with NaOAc to generate OAc$^-$ directly, avoiding the formation of surface trap states and achieving a J_{SC} value of 15.21 mA cm^{-2} in

a CsPbI$_3$ PNC solar cell without an antireflective coating.[107] Furthermore, the MeOAc treatment induced Cs vacancies due to the removal of bound Cs-oleate and the subsequent FAI post-treatment resulted in V_{OC} loss, allowing the PCE to remain at approximately 13%.[45,107] Instead of using FAI post-treatment, Ma et al. reported using a CsAc post-treatment that simultaneously improved the electronic coupling and filled the vacancies. Compared with the FAI-treated film, the CsAc-treated film demonstrated an improved carrier diffusion length (with similar carrier mobility but longer carrier lifetime) of 986 nm (Figure 5c). The final PCE was 14.10% with an improved J_{SC} ≈ 15 mA cm^{-2} and V_{OC} ≈ 1.25 V.[45]

Besides affecting the solid–liquid ligand exchange, ligand control during synthesis can improve the device performance, via ligand density management and ligand length reduction. The PNCs used for device fabrication are always synthesized using a hot-injection method with the long chain ligands OA and OLA. Ligand binding to the surface of PNCs is highly dynamic, allowing easy detachment during the purification process.[100] By taking the advantage of this property, the insulating ligand density around the PNCs can be controlled to promote electronic coupling. Although this method has proven to be feasible,[27] the loss of ligands introduces new problems such as stability and newly formed defects. Thus, subsequent treatments are required.

Based on a facile, hexane/MeOAc treatment, Liu et al. precisely controlled and quantified the ligand amount relating to the CsPbBrI$_2$ PNCs treatment and further systematically studied the impact of the ligand amount on the final device performance. Accompanied by the ligand loss, the PNCs gradually enlarged (Figure 5d). Without destroying the solubility, they controlled the ligand amount at 1.01 wt% to deposit the film following a simple annealing process, which induced partial crystal fusion and improved the interface properties between the PNCs. The device fabricated by PNCs with a low ligand amount exhibited a better film quality, improved carrier mobility, reduced trap states, and more efficient charge extraction compared to a device with a higher ligand amount. They achieved a high J_{SC} of 14.22 mA cm^{-2}, which was closest to the S–Q limit (86%) compared to other PNC solar cells. The final PCE was 12.2%, which was also the highest reported among mixed halide, inorganic PNC solar cells.[102] Although the annealing process reduced the interfaces between the PNCs by crystal fusion, this process is not suitable for all kinds of PNC solar cells, especially for CsPbI$_3$ and FAPbI$_3$, as the phase stability was attributed to the large contribution of the surface energy.[27,28] Yuan et al. applied a solution ligand exchange process to twice-purified CsPbI$_3$ PNCs. Ligands partially substituted with short chain phenyltrimethylammonium bromide (PTABr), which contains a benzene group, not only decreased the distance between the PNCs but also passivated the defects, resulting in an enhanced carrier mobility.[52]

In contrast to ligand exchange and other post-treatments, it is more promising to alter the initial ligands used in the synthesis of PNCs. Chen et al. successfully synthesized CsPbI$_3$ PNCs with excellent stability by partially replacing the OA/OLA ligands with octanoic/octylamine ligands. They further confirmed that shorter chain ligands exhibited much stronger adsorption onto the PNC surfaces than the long chain ligands, which suppressed
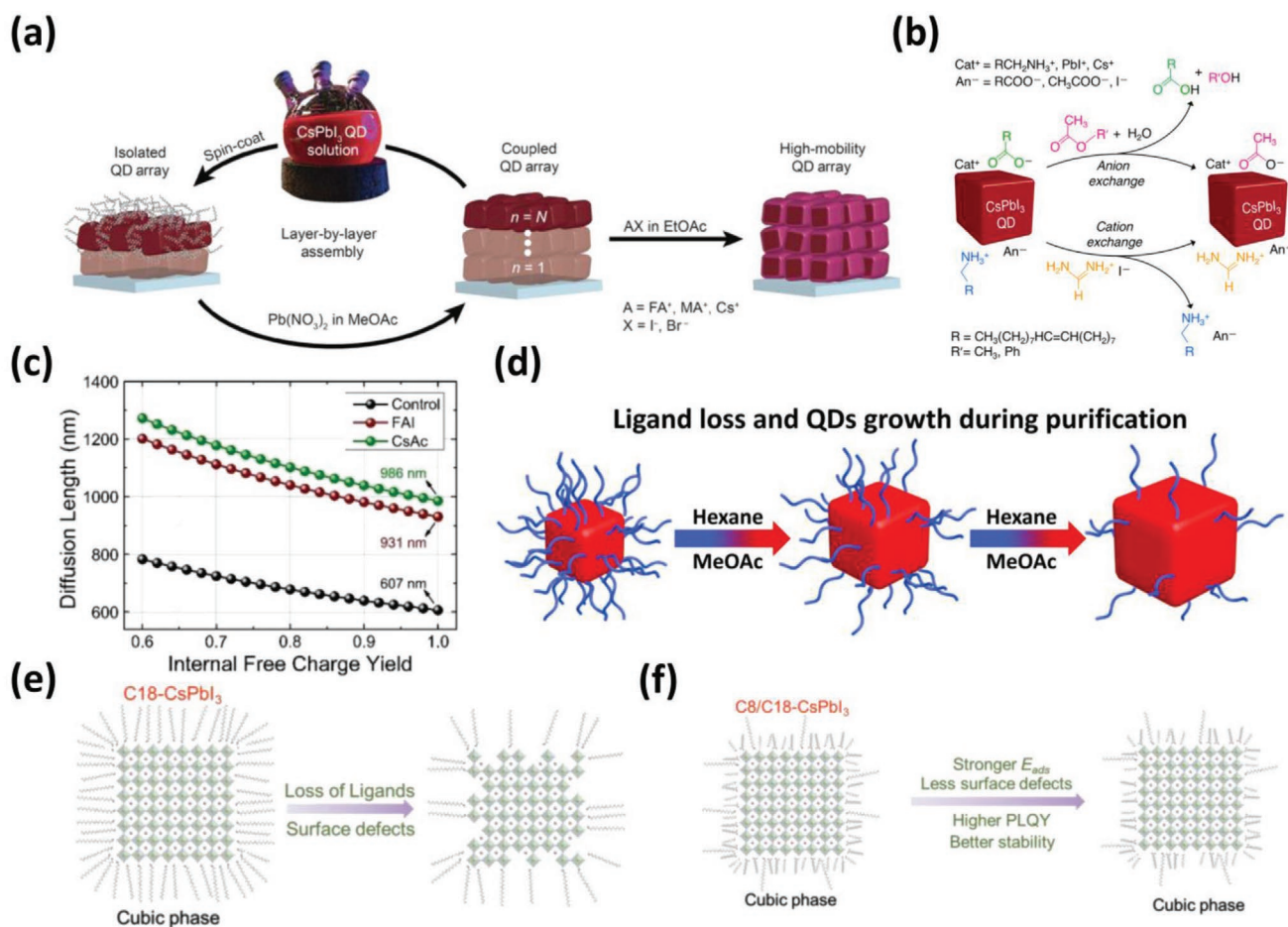
ADVANCED
SCIENCE NEWS
www.advancedsciencenews.com

small
methods
www.small-methods.com

Figure 5. a) Schematic of the film deposition process and AX salt post-treatment. Reproduced with permission.[51] Copyright 2017, American Association for the Advancement of Science. b) Schematic of the ligand exchange reaction during the two treatment processes. Reproduced with permission.[106] Copyright 2018, American Chemical Society. c) Free carrier diffusion length of PNC films calculated from the TRMC carrier mobility and lifetime values. Reproduced with permission.[45] Copyright 2019, Wiley-VCH. d) Illustration of the NC changes during hexane/MeOAc treatments. Reproduced with permission.[102] Copyright 2020, Wiley-VCH. Schematic of the stabilization mechanism and corresponding properties for: CsPbI$_3$ PNCs with e) long-chain ligands and f) short-chain ligands. Reproduced with permission.[108] Copyright 2019, Wiley-VCH.

defect formation due to the loss of ligands (Figure 5e,f). Thus, they achieved a high J_{SC} of 16.98 mA cm^{-2} in the CsPbI$_3$ PNC device.[108] In summary, various types of ligands have been used in the synthesis of PNCs, but the majority of ligands for PNCs used in solar cells have been limited to long chain OA/OLA. The use of other ligands should be investigated.

4.2.2. Additive Induced Cross-Linking

Due to the excellent processability of device fabrication, it is easy to adjust the active layer composition and enhance the device performance. Micrometer-sized graphene sheets (μGRs) possess extremely high electron mobility and can be modified using various functional groups that can interact with the surface of PNCs, including carbonyl and carboxyl.[109,110] By taking advantage of the μGR properties, Wang et al. used μGRs to crosslink the PNCs, which provided an extra charge transport channel. Thus, the crosslinked film exhibited accelerated charge extraction and reduced carrier recombination.

Simultaneously, the μGRs also protected the PNCs from agglomeration and moisture attack (**Figure 6**a–c).[111] However, direct contact with the hole transport layer also resulted in carrier recombination, which potentially accounted for the low performance improvement.[112] Taking this into account, Xue et al. adopted a conjugated, small, molecular 2,2′-[[6,6,12,12-tetrakis(4-hexylphenyl)-6,12-dihydrodithieno [2,3-d:2′,3′-d′]-s-indaceno[1,2-b:5,6-b′]dithiophene-2,8-diyl] bis[methylidyne(3-oxo-1H-indene-2,1(3H)-diylidene)]] bis[propanedinitrile] (ITIC) to enhance charge separation and transport via its controlled incorporation into a PNC film, where ITIC was mainly distributed in the film close to the electron transport layer rather evenly throughout the entire film (Figure 6d). Therefore, all of the performance parameters were significantly improved and the highest reported PCE of 12.7% in a FAPbI$_3$ PNC solar cell was demonstrated.[105] Inspired by heterostructures in traditional, hybrid, colloidal quantum dots/ organic solar cells, hybridization with conjugated polymers that possess various functional groups or atoms may also be a promising method for crosslinking PNCs.[37]
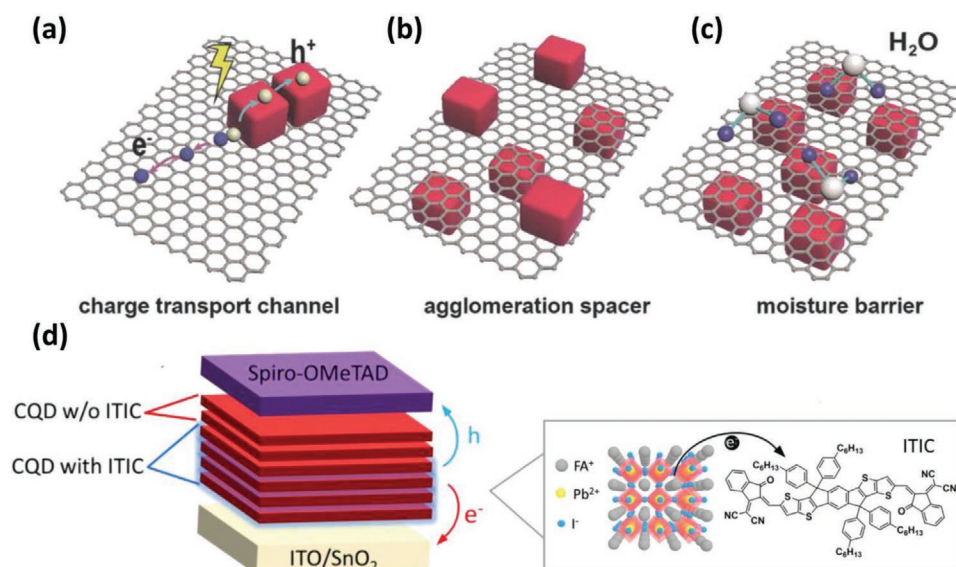
ADVANCED
SCIENCE NEWS
www.advancedsciencenews.com

small
methods
www.small-methods.com

Figure 6. Schematic drawing of the a) charge transport process and b,c) stabilization mechanism for the μGR/CsPbI3 film-based PNCs. Reproduced with permission.[111] Copyright 2018, Wiley-VCH. d) Schematic diagrams of FAPbI$_3$ PNC device structures where the ITIC distribution is controlled. Inset: chemical structure of ITIC. Reproduced with permission.[105] Copyright 2019, Wiley-VCH.

4.2.3. Device Interface Engineering

The strategies in Sections 4.2.1. and 4.2.2. discussed the direct or indirect enhancement of the coupling between PNCs, which leads to improved charge separation or transport, and thus more efficient charge extraction between interfaces. With regards to the device interface, an efficient extraction requires well-matched band alignment, good contact, excellent material properties, and PNC passivation.

Recently, Chen et al. incorporated CsPbI$_3$ PNCs into mesoporous TiO$_2$ (m-TiO$_2$) successfully using a CsOAc-saturated MeOAc solution during preprocessing (**Figure 7**a). Compared to the compact TiO$_2$ (c-TiO$_2$)-only based architecture, the architecture demonstrated more efficient charge separation, an increased electron extraction rate approximately two times higher, a J_{SC} of 17.77 mA cm^{-2} and a PCE of 14.32%, both of which are the highest reported in CsPbI$_3$ PNC devices.[113] Conjugated polymers have tremendous potential for charge extraction at the interface between PNCs and the hole transport layer. Zeng et al. demonstrated that the sulfur atoms of poly-3-hexylthiophene (P3HT) could passivate the interfacial, positively-charged, under-coordinated Cs$^+$ and suppress the formation of antisite defects by bonding to Pb (Figure 7b,c). They softened the P3HT to fill the spaces between interfaces by annealing, resulting in better contact. Moreover, annealing mitigated the energy disorder of P3HT. Due to the strong chemical interaction with the PNCs and good physical contact, efficient charge extraction was demonstrated.[48] Other polymers, such as poly[4,8-bis[(2-ethylhexyl) oxy]benzo[1,2-b:4,5-b']dithiophene-2,6-diyl-alt-3-fluoro-2-[(2-ethylhexyl)carbonyl]thieno[3,4-b]thiophene-4,6-diyl](PTB7) and poly[4,8-bis(5-(2-ethylhexyl)thiophen-2-yl)benzo[1,2-b;4.5b'] dithiophene-2,6-diyl-alt-3-fluoro-2-[(2-ethyl-hexyl)-carbonyl]-thieno[3,4-b]thiophene-4,6-diyl] (PTB7-th), were also studied in a CsPbI$_3$ PNC solar cell, reported by Ma et al. P3HT exhibited higher hole mobility compared to PTB7 and PTB7-Th but PTB7

exhibited more ideal charge extraction as shown in the lifetime histogram of time-resolved, confocal images (Figure 7d). The narrow lifetime histogram distribution suggested more effective defect passivation in the PTB7/PNCs and PTB7 demonstrated matched energy levels with CsPbI$_3$, indicating negligible band bending and barriers at the interface. More remarkably, both of the studies on polymer-based PNC solar cells reported not only an improved J_{SC} but also an extremely enhanced V_{OC}.[26]

Introducing a charge separation-assisted heterojunction inside the PNC absorber layer is a more direct and promising technique as it separates the charges where they are generated. By depositing PNCs with different energy levels in the unique layer-by-layer film fabrication process, as shown in Figure 7e, Zhao et al. controlled the thickness ratio of the bottom Cs$_X$FA$_{1-X}$ PbI$_3$ PNCs layers to the CsPbI$_3$ PNCs layers at 1:3. All devices with the heterojunction inside of the active layer demonstrated enhanced J_{SC} > 18 mA cm^{-2}, far exceeding that of pure CsPbI$_3$ PNCs at 15.75 mA cm^{-2}, and a PCE of 17.39% was achieved using a Cs$_{0.25}$FA$_{0.75}$PbI$_3$/CsPbI$_3$ heterojunction. The high J_{SC} could not be solely attributed to the enhanced charge separation induced by band alignment. The FA-containing PNCs with narrow bandgaps in the active layer also extended the light absorption range.[38] In this case, although a high J_{SC} was obtained, the device should be regarded as an FA-containing PNC solar cell with large room for improvement towards the S–Q limit.

Although the strategies discussed above have proven effective for performance improvement and large J_{SC} values have been realized, further improvements are still required to approach the S–Q limit.

5. Challenges

Despite their excellent properties and exciting progress, PNC solar cells still face serious challenges including their complex
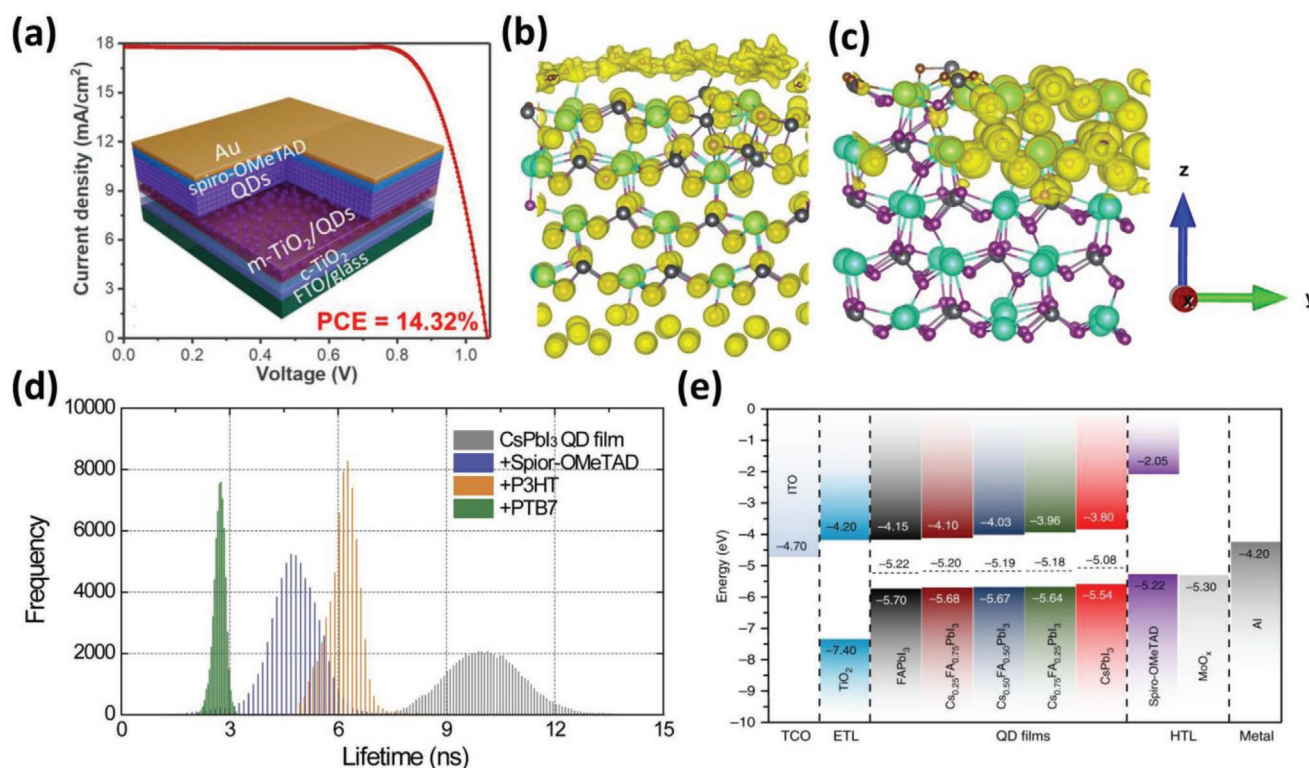
ADVANCED
SCIENCE NEWS
www.advancedsciencenews.com

small
methods
www.small-methods.com

Figure 7. a) Schematic view of $CsPbI_3$ PNC devices with mesoporous structures and the corresponding $J-V$ curve for the device with the best performance. Reproduced with permission.[113] Copyright 2020, American Chemical Society. Electron density distribution plots of b) P3HT and c) no P3HT on the $CsPbI_2Br$ 110-surface with antisite defects. Reproduced with permission.[48] Copyright 2018, Wiley-VCH. d) The lifetime histogram of the $CsPbI_3$ PNC film and $CsPbI_3$ PNC film with Spiro-OMeTAD, P3HT, and PTB7 on the top extracted from 2D lifetime images. Reproduced with permission.[26] Copyright 2018, Elsevier. e) Energy band positions for PNCs with various compositions and contact layers. The Fermi level positions are denoted by horizontal dotted lines. Reproduced with permission.[38] Copyright 2019, Springer Nature.

techniques, the toxicity of Pb, and poor stability, which impedes their further development and commercialization. Although pursuing superior device performance is attractive, these challenges should attract renewed focus and more attention should be paid to I-rich PNCs due to their appropriate bandgap.

5.1. Simplification of PNC Synthesis and Device Fabrication

Currently, the majority of PNCs used for solar cells are synthesized through hot injection methods. Although considerable progress has been made for hot injection methods on the laboratory scale, the nanocrystal size strongly depends on the reaction temperature. The temperatures of the reaction solution and injected precursor solution should be kept as consistent as possible, but this is hard to control.[20] High localization of injected precursors also leads to poor quality and dispersion of the PNCs when scaling up the fabrication process.[114] Thus, hot-injection methods with tedious preparation processes and inert gas protection cannot meet the requirements for large-scale and low-cost production and further commercial applications.[114,115]

Among the various reported synthesis methods for PNCs, ligand-assisted reprecipitation synthesis has been widely applied in LEDs, and meets the requirements for

rapid, facile, and scalable synthesis (**Figure 8**a).[114,115] In 2017, Akkerman et al. reported fast, room-temperature synthesis of $CsPbBr_3$ PNCs with environmentally friendly solvents and demonstrated their successful application in solar cells resulting in a high V_{OC} of 1.5 V and PCE of 5.4% (Figure 8b).[116] However, the film was fabricated by repeated deposition with no ligand or surface treatments, thus a higher PCE could be obtained after further optimization. The work is groundbreaking, but has not drawn significant attention in the field of PNC solar cells. Synthesized, Br-rich PNCs with large bandgaps are not appropriate for sunlight utilization. As for PNC solar cells with the desired $CsPbI_3$ composition, Dutta et al. reported that a high temperature was necessary for the synthesis of $CsPbI_3$ PNCs as it helps OLA ligands to occupy the surface Cs position and stabilize the PNCs.[117] Although the synthesis of PNCs with different components can be realized via an ion-exchange process, it undoubtedly complicates the procedures.[20,118] Recently, Polavarapu et al. synthesized $CsPbI_3$ nanoplatelets and $FAPbI_3$ nanocubes directly at room temperature using OA/OLA ligands. Interestingly, $CsPbI_3$ nanocubes were obtained when the reaction temperature increased to ≈80 °C. They proposed that there was a high energy barrier between the precursors and nanocubes.[119] The use of room temperature synthesized PNCs in solar cells is not impossible but potentially requires finding suitable ligands to modulate the synthesis of the PNCs.
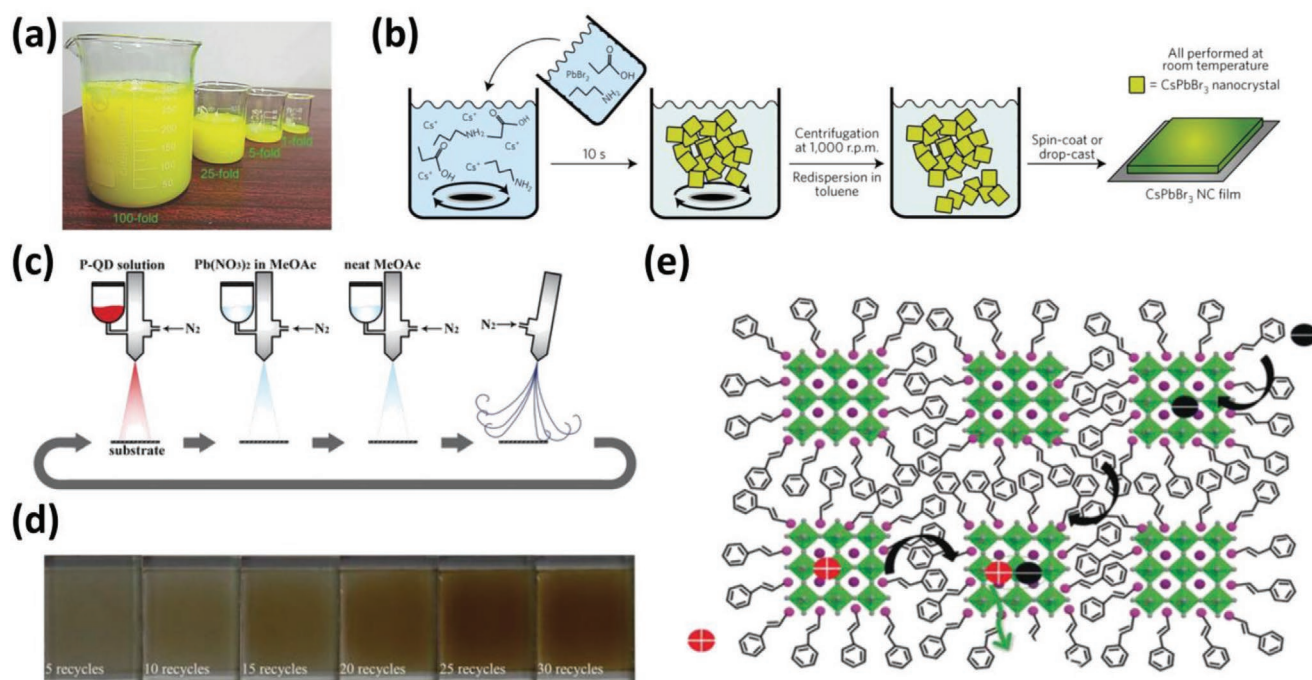
ADVANCED
SCIENCE NEWS
www.advancedsciencenews.com

small
methods
www.small-methods.com

Figure 8. a) Photograph of different scaled-up folds of a CsPbBr₃ PNC crude solution. Reproduced with permission.[115] Copyright 2018, Wiley-VCH. b) Schematic representation of the synthesis, where the PbBr₂ precursor solution is injected into a hexane/isopropanol mixture containing Cs⁺ cations. After centrifugation and redispersion in toluene, the inks can be directly used for fabrication of the films. Reproduced with permission.[116] Copyright 2016, Springer Nature. c) Process of spray-coating deposition and d) corresponding photographs of PNC thin films with different circulations. Reproduced with permission.[52] Copyright 2019, Wiley-VCH. e) Illustration of carrier transport in PNC films with conjugated ligands. Reproduced with permission.[120] Copyright 2018, Wiley-VCH.

Furthermore, their excellent processability ensures that PNCs are compatible with various processing technologies for achieving large-scale manufacturing and flexible-device processing. However, until now, the majority of studies on PNC solar cells have used layer-by-layer fabrication based on spin-coating. Yuan et al. attempted to fabricate PNC films using spray-coating technology (Figure 8c,d), achieving a PCE of 11.2% after a PTABr ligand exchange process.[52] The fabrication process was still a layer-by-layer method that required an additional ligand treatment. The critical point that made this an easier film fabrication process lies in the ligands anchored on the PNC surfaces. Conjugated ligands with high conductivity are ideal for process simplification and also maintain the PNC stability without sacrificing performance, which has been achieved for MAPbBr₃ PNC LEDs (Figure 8e).[120] The most promising strategy may be an in situ, synthesized approach during film fabrication without the synthesis of PNCs, as reported by Gao et al. They realized an in situ, synthesized, FAPbI₃ PNC film by spin-coating the precursor solution with aromatic ammonium iodide as ligands, where the size-dependent quantum confinement effect was adjusted by the subsequent annealing process.[121] This method was applied to solar cells, achieving a PCE of 13.4%.[122]

Simplification of the fabrication process of PNC solar cells is necessary for further development, in addition to the development of a facile PNC synthesis method and new film fabrication methods. Moreover, a facile fabrication technology for PNC solar cells will accelerate development.

5.2. Reducing Toxic Pb Consumption

Lead toxicity is a significant environmental problem although physical encapsulation can prevent Pb leakage.[123–125] For PNC solar cells, this is a serious problem because successful PNC synthesis requires a Pb-rich condition, typically requiring a high Pb/Cs molar feed ratio >4, and unreacted Pb-containing precursors are isolated during subsequent purification steps, which results in a significant amount of wasted Pb.[48,51] Thus, it is necessary for PNC solar cells to reduce the use of Pb. Liu et al. found that excess PbX₂ provided sufficient X⁻ to protect the PNCs from further reacting with Cs-oleate. Thus, they replaced a large amount of excess PbI₂ with GeI₂ to serve as the I⁻ source, lowering the Pb/Cs molar feed ratio to 0.66. Additionally, no Ge was incorporated into the PNCs and the corresponding solar cell exhibited a high PCE of 12.15%, which was comparable to a solar cell fabricated with conventionally synthesized PNCs.[126]

Another effective strategy for reducing Pb use is the partial or complete replacement of Pb. However, considering the final photovoltaic device performance, the Pb substitution must not degrade the material properties. Thus, it is difficult to find an ideal substitution for Pb and even harder to successfully incorporate it into the I-rich PNCs on account of fast nucleation.[127] Although various kinds of B-site doped PNCs have been reported, more attention should be paid to I-rich doped PNCs due to their appropriate bandgap for photovoltaic applications. Heterovalent substitutions possess poor electronic properties

due to reduction of the structural or electronic dimensionality, limiting device performance.[128] Bi[3+]-doped $CsPbI_3$ PNCs can introduce undesirable, in-gap trapping states, providing non-radiative channels.[129] A reported $CsPb_{0.9}Sb_{0.1}I_3$ PNC solar cell only exhibited a low PCE of 9.4% with enhanced stability.[130] However, Ma et al. realized Yb[3+] in situ doping in $CsPbI_3$ and achieved a PCE of 13.12% with reduced trapping states. A PCE of 12.27% was obtained when the molar feed ratio of Yb[3+]/Pb^{2+} was 50%.[131] For isovalent substitutions, Ge[2+] and Sn^{2+} both maintained the Pb^{2+}-like electronic features of a lone ns^2 pair of electrons and inactive p orbitals, exhibiting promising optoelectronic properties. Although the replacement of Pb with Sn induced a reduced bandgap and higher absorption coefficients, the potential for adverse effects including high Sn vacancies and easy oxidization of Sn^{2+} to Sn^{4+} should also be considered.[132] Ge substitution faces similar problems regarding oxidation and the low enthalpy of formation of Ge

vacancies.[128] Currently, PNC solar cells without Pb demonstrate PCE values as high as 12.96%, which was achieved using $CsSnI_3$ nanorods, but the fabrication process must avoid oxygen and moisture.[133] Mn^{2+} is a potentially promising candidate for replacing Pb as it has been theoretically and experimentally proved that, except for the enhanced stability, there are no property differences between Mn-alloyed $CsPbI_3$ PNCs and pure $CsPbI_3$ PNCs. This is because the localized electronic states of the Mn orbitals make a negligible contribution to the electronic structure (**Figure 9**a). Calculations have indicated that the Mn:Pb ratio of Mn-alloyed $CsPbI_3$ PNCs can be up to 1:1 but an initial feed ratio of Pb:Mn = 2:1 only results in 10% alloying. Nevertheless, this is enough to lower the Pb/Cs molar feed ratio to ≈2.6.[127] Other successful alloys using B-site ions in I-rich PNCs have been reported such as Zn^{2+}, Sr^{2+}, and Gd^{3+}, which require further research into their electronic properties and device performance.[134–136]
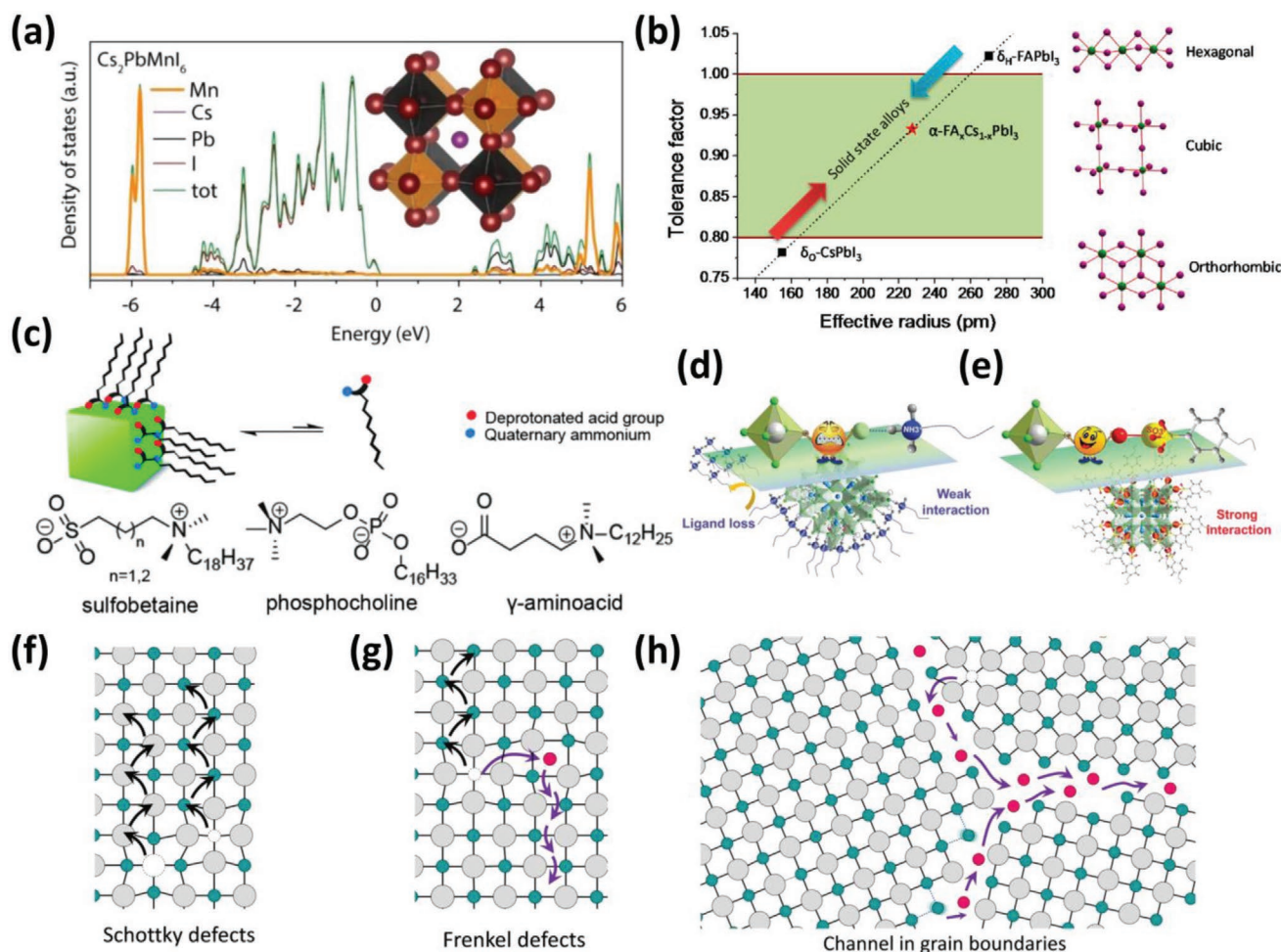

Figure 9. a) The projected density of states calculated at the HSE06 level by including spin orbit corrections of the most stable cubic Cs_2PbMnI_6 system. Reproduced with permission.[127] Copyright 2017, American Chemical Society. b) Correlations between the tolerance factor and crystal structure of perovskite materials. Reproduced with permission.[137] Copyright 2016, American Chemical Society. c) Examples of long-chain sulfobetaines, phosphocholines, and γ-amino acids are depicted left to right (n = 1): 3-(N,N-dimethyloctadecylammonio)-propanesulfonate, N-hexadecylphosphocholine, and N,N-dimethyldodecylammoniumbutyrate. Reproduced with permission.[142] Copyright 2018, American Chemical Society. Bonding motif on the PNC surfaces and interaction strength of d) OLA and e) dodecylbenzene sulfonic acid. Reproduced with permission.[7] Copyright 2019, Wiley-VCH. Illustration of the ion migration pathways enabled by f) Schottky defects, g) Frenkel defects, and h) open space and wrong bonds at grain boundaries. Reproduced with permission.[153] Copyright 2016, American Chemical Society.

**ADVANCED
SCIENCE NEWS**

www.advancedsciencenews.com

**small
methods**

www.small-methods.com

5.3. Stability Improvement

Both bulk $CsPbI_3$ and $FAPbI_3$ materials easily transform to the non-perovskite phase at room temperature (Figure 9b).[137] Although PNCs are relatively stable due to the large contribution of their surface energy,[27,28] PNCs can still lose their phase and colloidal stability during purification or storage, influencing the device performance. This problem is exacerbated when PNCs are exposed to polar solvents or an ambient atmosphere with a combination of light, moisture, and temperature.[7,31,96,98,100] In addition, improved device performance requires atmospheric control, especially moisture control, during the film fabrication and purification.[138] When PNCs are assembled into the active layer, aside from the influence of ambient atmosphere, they also suffer additional harsh conditions during operation or measurement. The stability issues of PNC solar cells must be urgently overcome for further development and commercialization.

5.3.1. Phase Stability

The poor phase stability of $CsPbI_3$ and $FAPbI_3$ originates from the improper A cation size. The suitability of the A cation fitting within the cuboctahedral void formed from the $[PbX_3]^-$ octahedral sublattice can be assessed by the Goldschmidt tolerance factor (t), which is defined as

$$t = \frac{r_A + r_x}{\sqrt{2}(r_B + r_x)} \tag{7}$$

where r_A, r_B, and r_X are the effective ionic radii of the A, B, and X cations, respectively. Between $0.8 \leq t \leq 1$, perovskite phase formation is favorable, but for $t < 0.9$, the perovskite structure is distorted due to the tilted $[PbX_3]^-$ octahedral.[57,139,140] For $APbI_3$, both Cs^+ and FA^+ are improperly sized, resulting in undesirable factors for $CsPbI_3$ ($t = 0.89$) and $FAPbI_3$ ($t = 1.03$).[57] Doping or alloying other ions can modulate the value of t and, along with the impact on cohesive energy and lattice contraction, further help stabilize the PNCs.[127,134,135] However, the stability improvement cannot be at the expense of device performance. Successful doping or alloying should not play a harmful role in the electronic structure. When the X-site was alloyed with smaller Br^-, this resulted in an increased bandgap, fast carrier recombination, and poor charge transport.[49] B-site alloying, discussed in Section 5.2., using small Mn^{2+} or Sn^{2+} is feasible. Interestingly, alloyed $CsSn_{1-X}Pb_XI_3$ PNCs form a new crystal structure and exhibit excellent long-term stability, superior to their parents ($CsSnI_3$ and $CsPbI_3$ PNCs), whether in solution or in film. However, for achieving a high device performance, it is necessary to reduce the large density of trap states induced by Sn vacancies.[141] As for the A-site, $FA_{1-X}Cs_XPbI_3$ can increase the phase stability and optimize the electronic structure and optoelectronic properties, which is promising for future research, as discussed in Section 2.4.

5.3.2. Colloidal Stability

Similar to the highly soft bonds inside PNCs, the external bonds with ligands are highly dynamic, inducing colloidal instability

during purification and even long-term storage via inert gas protection.[7,31,100] The destruction of colloidal stability causes agglomeration and, consequently, an undesirable phase transformation.[44] Moreover, the detachment of ammonium ligands along with X^- or in the form of oleylammonium oleate exposes traps on the PNC surfaces, influencing their optoelectronic properties and the device performance.[95] For I-rich components, this problem is exacerbated because I^- interacts more weakly with OLA than other X^- components.[28] Therefore, $CsPbI_3$ PNCs are more sensitive to polar solvents during the purification and isolation processes. By using MeOAc as the antisolvent, Luther et al. successfully isolated $CsPbI_3$ PNCs that were stable enough for device fabrication and further characterization. However, they also found that the esters hydrolyzed with the atmospheric moisture absorbed onto the PNC surfaces, changing the surface properties. In other words, the device performance of the ester-purified PNCs was highly dependent on the environmental humidity.[28,106] Although many groups have applied esters as antisolvents, esters might not be the most appropriate antisolvents and further exploration is required. Regardless of the chosen antisolvent, the root of the poor colloidal stability is the highly dynamic bonding ligands. PNCs that are tightly bonded with other ligands should be considered for use in solar cells. Kovalenko et al. successfully synthesized more stable PNCs using zwitterionic molecules as multidentate ligands because the chelate effect helped the ligands to firmly bind to the PNC surfaces (Figure 9c).[142] Considering that ammonium interacts with halides on the PNC surfaces through hydrogen bonding, Yang et al. proposed that hydrogen bonding weakened the Coulomb interaction between X and Pb, resulting in detachment (Figure 9d). Thus, they replaced the OA/OLA ligands with dodecylbenzene sulfonic acid that bonded with Pb and stabilized the PNCs (Figure 9e). The diffusion coefficient of the sulfonic-capped PNCs in solution was $121\ \mu m^2\ s^{-1}$, which was much lower than that of the OLA-capped PNCs ($166\ \mu m^2\ s^{-1}$), indicating much stronger interaction. The dispersity and optical properties of the sulfonic-capped PNCs remained unchanged after eight purification cycles.[7] Instead of hindering ligand detachment, ligand detachment can be seen as an advantage, which enables the modification of PNC surfaces with short ligands, such as phenethylammonium halide, 2,2′-iminodibenzoic acid (bidentate ligand), and thiocyanate, to simultaneously stabilize the PNCs and improve the final device performance[54,143–145]

5.3.3. Operational Stability

Instability induced by atmospheric conditions can be avoided by excellent encapsulation, but encapsulation cannot prevent undesirable, internal changes.[146,147] When perovskite devices are under operation, light illumination and electric field changes induce ion migration towards the interfaces due to the low formation energy of the perovskite lattice.[146,148–151] Ion migration causes device degradation, hysteresis, and phase segregation for mixed-halide perovskites.[152] It is widely accepted that grain boundaries and defects are extremely important channels for ion migration (Figure 9f–h).[149,153,154] Although PNCs are capped by ligands, they are largely removed during the purification or device fabrication stages, resulting in surface

**ADVANCED
SCIENCE NEWS**
www.advancedsciencenews.com

**small
methods**
www.small-methods.com

vacancy defects.[27] Moreover, the small size and large surface area of the PNCs greatly amplifies defects on the grain boundaries.[155] Therefore, ion migration occurs more drastically and has been observed in PNC-based devices.[150,156–159] Despite research remaining limited regarding ion migration in PNC solar cells, this does not mean that ion migration is minor, as there is an obvious ion migration-related hysteresis.[48,102,107] For example, the highest PCE achieved for PNC solar cells is 17.39% by reverse-scanning, while only a low PCE of 11.46% has been achieved through forward scanning.[38] Other urgent challenges in PNC solar cells may currently attract more attention, but ion migration must be resolved. Strategies can be developed from PNC LEDs, where ion migration is more serious due to the larger electric field.[160] Passivation of surface halide vacancies and crosslinking are promising techniques.[157–160]

6. Conclusions and Considerations

As an emerging material for use in solar cells, PNCs have shown significant development in recent years. Despite current achievements, there is still substantial, untapped potential in the field. Although the device performance of PNCs requires further improvement, more studies should focus on the PNCs themselves. In our view, the following five points require deep consideration:

First, what is the best component for PNC solar cells?

$APbI_3$ PNCs possess an ideal bandgap but suffer from instability due to their improper Goldschmidt tolerance factor. While Br-alloying can alleviate the problem, this results in a large bandgap and poor charge dynamics and substitution with other ions may affect the electronic structure. Mixing Cs and FA on the A-site not only enhances the phase stability but also optimizes the optoelectronic properties, as discussed in Sections 2.2. and 2.4. Thus, $Cs_XFA_{1-X}PbI_3$ PNCs are the most promising for solar cell fabrication and deserve more attention.

Second, what is the best choice of B-site doping or alloying for a PNC device?

As we have discussed in Sections 5.2. and 5.3.1., ideal alloying or doping not only reduces the consumption of toxic Pb but also improves the stability and properties. Although various ions have been successfully used for doping or alloying in PNCs, their respective impacts on the electronic properties and corresponding device performance of PNCs still require systematic study.

Third, what is the best ligand choice for PNCs?

Ligands play an extremely critical role in various aspects of PNCs, such as their stability, final device performance, and even the synthesis and device fabrication process. Although OA/OLA ligand pairs have been adopted to synthesize PNCs in the majority of studies regarding PNC solar cells, they are highly dynamic and imprison the charges, resulting in complications. Other short or conjugated ligands with stronger interactions with PNCs should be explored. Although direct synthesis using new-type ligands may be difficult, facile ligand postexchange treatments are also viable options.

Fourth, how to improve the contribution of hot carriers or multiple excitons to the device?

Although, currently, the most urgent demand for PNC solar cells is to improve the device performance, this cannot overshadow their potential to surpass the Shockley–Queisser limit.

Thus, as with lead chalcogenides and traditional quantum dots, hot carriers and multiple exciton generation in PNCs should be further investigated, particularly regarding their efficient utilization.

Fifth, are hot-injection synthesized PNCs the best choice for device fabrication?

The majority of PNC solar cells use hot-injection methods, which are satisfactory for lab-scale research, but these complicated processes may limit commercial applications, as discussed in Section 5.1. Ligand-assisted reprecipitation is a promising technique for simplifying PNC synthesis. Furthermore, nanosize, I-rich PNCs self-stabilize due to their large surface energy. From this point of view, spin-coating the precursor with ligands to synthesize PNCs in situ deserves further investigation in solar cells.

All in all, the various challenges and deficiencies of PNCs cannot overshadow their potential as a promising photovoltaic material due to their excellent and unique properties. The key is determining how to exploit these properties. We predict that PNCs will attract increasing attention in the near future and become an emerging star in the field of photovoltaic research.

Conflict of Interest

The authors declare no conflict of interest.

Keywords

[1] W. Hu, H. Cong, W. Huang, Y. Huang, L. Chen, A. Pan, C. Xue, *Light: Sci. Appl.* **2019**, *8*, 106.

[2] C. Li, H. Wang, F. Wang, T. Li, M. Xu, H. Wang, Z. Wang, X. Zhan, W. Hu, L. Shen, *Light: Sci. Appl.* **2020**, *9*, 31.

[3] L. Gu, Z. Fan, *Light: Sci. Appl.* **2017**, *6*, e17090.

[4] S. B. Kang, J. H. Kim, M. H. Jeong, A. Sanger, C. U. Kim, C. M. Kim, K. J. Choi, *Light: Sci. Appl.* **2019**, *8*, 121.

[5] H. W. Chen, R. D. Zhu, J. He, W. Duan, W. Hu, Y. Q. Lu, M. C. Li, S. L. Lee, Y. J. Dong, S. T. Wu, *Light: Sci. Appl.* **2017**, *6*, e17043.

[6] K. K. Liu, Q. Liu, D. W. Yang, Y. C. Liang, L. Z. Sui, J. Y. Wei, G. W. Xue, W. B. Zhao, X. Y. Wu, L. Dong, C. X. Shan, *Light: Sci. Appl.* **2020**, *9*, 44.

**ADVANCED
SCIENCE NEWS**

www.advancedsciencenews.com

**small
methods**

www.small-methods.com

[7] D. Yang, X. Li, W. Zhou, S. Zhang, C. Meng, Y. Wu, Y. Wang, H. Zeng, *Adv. Mater.* **2019**, *31*, 1900767.

[8] H. Sun, Z. Yang, M. Wei, W. Sun, X. Li, S. Ye, Y. Zhao, H. Tan, E. L. Kynaston, T. B. Schon, H. Yan, Z. H. Lu, G. A. Ozin, E. H. Sargent, D. S. Seferos, *Adv. Mater.* **2017**, *29*, 1701153.

[9] Q. Dong, Y. Fang, Y. Shao, P. Mulligan, J. Qiu, L. Cao, J. Huang, *Science* **2015**, *347*, 967.

[10] H. Wei, D. DeSantis, W. Wei, Y. Deng, D. Guo, T. J. Savenije, L. Cao, J. Huang, *Nat. Mater.* **2017**, *16*, 826.

[11] Y. Miao, L. Cheng, W. Zou, L. Gu, J. Zhang, Q. Guo, Q. Peng, M. Xu, Y. He, S. Zhang, Y. Cao, R. Li, N. Wang, W. Huang, J. Wang, *Light: Sci. Appl.* **2020**, *9*, 89.

[12] H. H. Fang, F. Wang, S. Adjokatse, N. Zhao, J. Even, M. Antonietta Loi, *Light: Sci. Appl.* **2016**, *5*, e16056.

[13] H. Wei, Y. Fang, P. Mulligan, W. Chuirazzi, H.-H. Fang, C. Wang, B. R. Ecker, Y. Gao, M. A. Loi, L. Cao, J. Huang, *Nat. Photonics* **2016**, *10*, 333.

[14] H. Wei, J. Huang, *Nat. Commun.* **2019**, *10*, 1066.

[15] C. Xie, P. You, Z. Liu, L. Li, F. Yan, *Light: Sci. Appl.* **2017**, *6*, e17023.

[16] J. Xing, C. Zhao, Y. Zou, W. Kong, Z. Yu, Y. Shan, Q. Dong, D. Zhou, W. Yu, C. Guo, *Light: Sci. Appl.* **2020**, *9*, 111.

[17] L. C. Schmidt, A. Pertegás, S. González-Carrero, O. Malinkiewicz, S. Agouram, G. Mínguez Espallargas, H. J. Bolink, R. E. Galian, J. Pérez-Prieto, *J. Am. Chem. Soc.* **2014**, *136*, 850.

[18] V. Babin, P. Fabeni, M. Nikl, G. Pazzi, I. Sildos, N. Zazubovich, S. Zazubovich, *Chem. Phys. Lett.* **1999**, *314*, 31.

[19] L. Protesescu, S. Yakunin, M. I. Bodnarchuk, F. Krieg, R. Caputo, C. H. Hendon, R. X. Yang, A. Walsh, M. V. Kovalenko, *Nano Lett.* **2015**, *15*, 3692.

[20] S. Wei, Y. Yang, X. Kang, L. Wang, L. Huang, D. Pan, *Chem. Commun.* **2016**, *52*, 7265.

[21] G.-L. Yang, H.-Z. Zhong, *Chin. Chem. Lett.* **2016**, *27*, 1124.

[22] K. Yang, F. Li, Y. Liu, Z. Xu, Q. Li, K. Sun, L. Qiu, Q. Zeng, Z. Chen, W. Chen, W. Lin, H. Hu, T. Guo, *ACS Appl. Mater. Interfaces* **2018**, *10*, 27374.

[23] M. Chen, Y. Zou, L. Wu, Q. Pan, D. Yang, H. Hu, Y. Tan, Q. Zhong, Y. Xu, H. Liu, B. Sun, Q. Zhang, *Adv. Funct. Mater.* **2017**, *27*, 1701121.

[24] H. Liu, Z. Wu, H. Gao, J. Shao, H. Zou, D. Yao, Y. Liu, H. Zhang, B. Yang, *ACS Appl. Mater. Interfaces* **2017**, *9*, 42919.

[25] Z. Y. Zhu, Q. Q. Yang, L. F. Gao, L. Zhang, A. Y. Shi, C. L. Sun, Q. Wang, H. L. Zhang, *J. Phys. Chem. Lett.* **2017**, *8*, 1610.

[26] J. Yuan, X. Ling, D. Yang, F. Li, S. Zhou, J. Shi, Y. Qian, J. Hu, Y. Sun, Y. Yang, X. Gao, S. Duhm, Q. Zhang, W. Ma, *Joule* **2018**, *2*, 2450.

[27] J. Xue, J.-W. Lee, Z. Dai, R. Wang, S. Nuryyeva, M. E. Liao, S.-Y. Chang, L. Meng, D. Meng, P. Sun, O. Lin, M. S. Goorsky, Y. Yang, *Joule* **2018**, *2*, 1866.

[28] A. Swarnkar, A. R. Marshall, E. M. Sanehira, B. D. Chernomordik, D. T. Moore, J. A. Christians, T. Chakrabarti, J. M. Luther, *Science* **2016**, *354*, 92.

[29] A. Swarnkar, R. Chulliyil, V. K. Ravi, M. Irfanullah, A. Chowdhury, A. Nag, *Angew. Chem., Int. Ed.* **2015**, *54*, 15424.

[30] Q. A. Akkerman, G. Rainò, M. V. Kovalenko, L. Manna, *Nat. Mater.* **2018**, *17*, 394.

[31] M. V. Kovalenko, L. Protesescu, M. I. Bodnarchuk, *Science* **2017**, *358*, 745.

[32] X. Zhu, L. Bian, H. Fu, L. Wang, B. Zou, Q. Dai, J. Zhang, H. Zhong, *Light: Sci. Appl.* **2020**, *9*, 73.

[33] J. Song, J. Li, X. Li, L. Xu, Y. Dong, H. Zeng, *Adv. Mater.* **2015**, *27*, 7162.

[34] Y. Wang, X. Li, J. Song, L. Xiao, H. Zeng, H. Sun, *Adv. Mater.* **2015**, *27*, 7101.

[35] C. H. Kang, I. Dursun, G. Liu, L. Sinatra, X. Sun, M. Kong, J. Pan, P. Maity, E. N. Ooi, T. K. Ng, O. F. Mohammed, O. M. Bakr, B. S. Ooi, *Light: Sci. Appl.* **2019**, *8*, 94.

[36] P. Ramasamy, D. H. Lim, B. Kim, S. H. Lee, M. S. Lee, J. S. Lee, *Chem. Commun.* **2016**, *52*, 2067.

[37] S.-W. Baek, S. Jun, B. Kim, A. H. Proppe, O. Ouellette, O. Voznyy, C. Kim, J. Kim, G. Walters, J. H. Song, S. Jeong, H. R. Byun, M. S. Jeong, S. Hoogland, F. P. García de Arquer, S. O. Kelley, J.-Y. Lee, E. H. Sargent, *Nat. Energy* **2019**, *4*, 969.

[38] Q. Zhao, A. Hazarika, X. Chen, S. P. Harvey, B. W. Larson, G. R. Teeter, J. Liu, T. Song, C. Xiao, L. Shaw, *Nat. Commun.* **2019**, *10*, 1.

[39] National Renewable Energy Laboratory, Best Research-Cell Efficiency Chart, https://www.nrel.gov/pv/device-performance.html (accessed: June 2020).

[40] W. Chen, H. Chen, G. Xu, R. Xue, S. Wang, Y. Li, Y. Li, *Joule* **2019**, *3*, 191.

[41] B. Yu, H. Zhang, J. Wu, Y. Li, H. Li, Y. Li, J. Shi, H. Wu, D. Li, Y. Luo, Q. Meng, *J. Mater. Chem. A* **2018**, *6*, 19810.

[42] D. Bai, H. Bian, Z. Jin, H. Wang, L. Meng, Q. Wang, S. Liu, *Nano Energy* **2018**, *52*, 408.

[43] L. Zhang, B. Li, J. Yuan, M. Wang, T. Shen, F. Huang, W. Wen, G. Cao, J. Tian, *J. Phys. Chem. Lett.* **2018**, *9*, 3646.

[44] J. K. Nam, M. S. Jung, S. U. Chai, Y. J. Choi, D. Kim, J. H. Park, *J. Phys. Chem. Lett.* **2017**, *8*, 2936.

[45] X. Ling, S. Zhou, J. Yuan, J. Shi, Y. Qian, B. W. Larson, Q. Zhao, C. Qin, F. Li, G. Shi, C. Stewart, J. Hu, X. Zhang, J. M. Luther, S. Duhm, W. Ma, *Adv. Energy Mater.* **2019**, *9*, 1900721.

[46] M. Cong, B. Yang, J. Chen, F. Hong, S. Yang, W. Deng, K. Han, *J. Phys. Chem. Lett.* **2020**, *11*, 1921.

[47] S. Zhang, S. Wu, W. Chen, H. Zhu, Z. Xiong, Z. Yang, C. Chen, R. Chen, L. Han, W. Chen, *Mater. Today Energy* **2018**, *8*, 125.

[48] Q. Zeng, X. Zhang, X. Feng, S. Lu, Z. Chen, X. Yong, S. A. T. Redfern, H. Wei, H. Wang, H. Shen, W. Zhang, W. Zheng, H. Zhang, J. S. Tse, B. Yang, *Adv. Mater.* **2018**, *30*, 1705393.

[49] M. Suri, A. Hazarika, B. W. Larson, Q. Zhao, M. Vallés-Pelarda, T. D. Siegler, M. K. Abney, A. J. Ferguson, B. A. Korgel, J. M. Luther, *ACS Energy Lett.* **2019**, *4*, 1954.

[50] C. de Weerd, L. Gomez, A. Capretti, D. M. Lebrun, E. Matsubara, J. Lin, M. Ashida, F. C. M. Spoor, L. D. A. Siebbeles, A. J. Houtepen, K. Suenaga, Y. Fujiwara, T. Gregorkiewicz, *Nat. Commun.* **2018**, *9*, 4199.

[51] E. M. Sanehira, A. R. Marshall, J. A. Christians, S. P. Harvey, P. N. Ciesielski, L. M. Wheeler, P. Schulz, L. Y. Lin, M. C. Beard, J. M. Luther, *Sci. Adv.* **2017**, *3*, eaao4204.

[52] J. Yuan, C. Bi, S. Wang, R. Guo, T. Shen, L. Zhang, J. Tian, *Adv. Funct. Mater.* **2019**, *29*, 1906615.

[53] H. J. Queisser, E. E. Haller, *Science* **1998**, *281*, 945.

[54] B. A. Koscher, J. K. Swabeck, N. D. Bronstein, A. P. Alivisatos, *J. Am. Chem. Soc.* **2017**, *139*, 6566.

[55] J. Kang, L.-W. Wang, *J. Phys. Chem. Lett.* **2017**, *8*, 489.

[56] A. Buin, P. Pietsch, J. Xu, O. Voznyy, A. H. Ip, R. Comin, E. H. Sargent, *Nano Lett.* **2014**, *14*, 6281.

[57] H. Huang, M. I. Bodnarchuk, S. V. Kershaw, M. V. Kovalenko, A. L. Rogach, *ACS Energy Lett.* **2017**, *2*, 2071.

[58] R. E. Brandt, V. Stevanović, D. S. Ginley, T. Buonassisi, *MRS Commun.* **2015**, *5*, 265.

[59] R. E. Brandt, J. R. Poindexter, P. Gorai, R. C. Kurchin, R. L. Z. Hoye, L. Nienhaus, M. W. B. Wilson, J. A. Polizzotti, R. Sereika, R. Žaltauskas, L. C. Lee, J. L. MacManus-Driscoll, M. Bawendi, V. Stevanović, T. Buonassisi, *Chem. Mater.* **2017**, *29*, 4667.

[60] K. Miyata, D. Meggiolaro, M. T. Trinh, P. P. Joshi, E. Mosconi, S. C. Jones, F. De Angelis, X.-Y. Zhu, *Sci. Adv.* **2017**, *3*, e1701217.

[61] K. Miyata, T. L. Atallah, X.-Y. Zhu, *Sci. Adv.* **2017**, *3*, e1701469.

[62] A. A. Bakulin, O. Selig, H. J. Bakker, Y. L. Rezus, C. Muller, T. Glaser, R. Lovrincic, Z. Sun, Z. Chen, A. Walsh, J. M. Frost, T. L. Jansen, *J. Phys. Chem. Lett.* **2015**, *6*, 3663.

[63] S. S. Lim, D. Giovanni, Q. Zhang, A. Solanki, N. F. Jamaludin, J. W. M. Lim, N. Mathews, S. Mhaisalkar, M. S. Pshenichnikov, T. C. Sum, *Sci. Adv.* **2019**, *5*, eaax3620.

[64] J. Fu, Q. Xu, G. Han, B. Wu, C. H. A. Huan, M. L. Leek, T. C. Sum, *Nat. Commun.* **2017**, *8*, 1300.

[65] R. T. Ross, A. J. Nozik, *J. Appl. Phys.* **1982**, *53*, 3813.

[66] H. Zhu, K. Miyata, Y. Fu, J. Wang, P. P. Joshi, D. Niesner, K. W. Williams, S. Jin, X.-Y. Zhu, *Science* **2016**, *353*, 1409.

[67] Y. Yang, D. P. Ostrowski, R. M. France, K. Zhu, J. van de Lagemaat, J. M. Luther, M. C. Beard, *Nat. Photonics* **2016**, *10*, 53.

[68] H.-H. Fang, S. Adjokatse, S. Shao, J. Even, M. A. Loi, *Nat. Commun.* **2018**, *9*, 243.

[69] J. Hayes, A. Levi, *IEEE J. Quantum Electron.* **1986**, *22*, 1744.

[70] M. Bernardi, D. Vigil-Fowler, J. Lischner, J. B. Neaton, S. G. Louie, *Phys. Rev. Lett.* **2014**, *112*, 257402.

[71] D. J. Suntrup, G. Gupta, H. Li, S. Keller, U. K. Mishra, *Appl. Phys. Lett.* **2014**, *105*, 263506.

[72] Z. Guo, Y. Wan, M. Yang, J. Snaider, K. Zhu, L. Huang, *Science* **2017**, *356*, 59.

[73] M. Li, S. Bhaumik, T. W. Goh, M. S. Kumar, N. Yantara, M. Grätzel, S. Mhaisalkar, N. Mathews, T. C. Sum, *Nat. Commun.* **2017**, *8*, 14350.

[74] S. Sarkar, V. K. Ravi, S. Banerjee, G. R. Yettapu, G. B. Markad, A. Nag, P. Mandal, *Nano Lett.* **2017**, *17*, 5402.

[75] M. Li, R. Begum, J. Fu, Q. Xu, T. M. Koh, S. A. Veldhuis, M. Gratzel, N. Mathews, S. Mhaisalkar, T. C. Sum, *Nat. Commun.* **2018**, *9*, 4197.

[76] M. C. Hanna, A. J. Nozik, *J. Appl. Phys.* **2006**, *100*, 074510.

[77] S. Saeed, C. de Weerd, P. Stallinga, F. C. M. Spoor, A. J. Houtepen, L. Da Siebbeles, T. Gregorkiewicz, *Light: Sci. Appl.* **2015**, *4*, e251.

[78] O. E. Semonin, J. M. Luther, S. Choi, H.-Y. Chen, J. Gao, A. J. Nozik, M. C. Beard, *Science* **2011**, *334*, 1530.

[79] M. L. Bohm, T. C. Jellicoe, M. Tabachnyk, N. J. Davis, F. Wisnivesky-Rocca-Rivarola, C. Ducati, B. Ehrler, A. A. Bakulin, N. C. Greenham, *Nano Lett.* **2015**, *15*, 7987.

[80] N. J. L. K. Davis, M. L. Böhm, M. Tabachnyk, F. Wisnivesky-Rocca-Rivarola, T. C. Jellicoe, C. Ducati, B. Ehrler, N. C. Greenham, *Nat. Commun.* **2015**, *6*, 8259.

[81] H. Goodwin, T. C. Jellicoe, N. J. L. K. Davis, M. L. Böhm, *Nanophotonics* **2018**, *7*, 111.

[82] M. C. Beard, J. M. Luther, O. E. Semonin, A. J. Nozik, *Acc. Chem. Res.* **2013**, *46*, 1252.

[83] M. C. Beard, A. G. Midgett, M. C. Hanna, J. M. Luther, B. K. Hughes, A. J. Nozik, *Nano Lett.* **2010**, *10*, 3019.

[84] A. Hazarika, Q. Zhao, E. A. Gaulding, J. A. Christians, B. Dou, A. R. Marshall, T. Moot, J. J. Berry, J. C. Johnson, J. M. Luther, *ACS Nano* **2018**, *12*, 10327.

[85] S. Rühle, *Sol. Energy* **2016**, *130*, 139.

[86] C. Liu, Q. Zeng, B. Yang, *Adv. Mater. Interfaces* **2019**, *6*, 1901136.

[87] M. Hao, Y. Bai, S. Zeiske, L. Ren, J. Liu, Y. Yuan, N. Zarrabi, N. Cheng, M. Ghasemi, P. Chen, M. Lyu, D. He, J.-H. Yun, Y. Du, Y. Wang, S. Ding, A. Armin, P. Meredith, G. Liu, H.-M. Cheng, L. Wang, *Nat. Energy* **2020**, *5*, 79.

[88] L. Wang, C. McCleese, A. Kovalsky, Y. Zhao, C. Burda, *J. Am. Chem. Soc.* **2014**, *136*, 12205.

[89] S. Chen, X. Wen, J. S. Yun, S. Huang, M. Green, N. J. Jeon, W. S. Yang, J. H. Noh, J. Seo, S. I. Seok, A. Ho-Baillie, *ACS Appl. Mater. Interfaces* **2017**, *9*, 6072.

[90] V. Kapoor, A. Bashir, L. J. Haur, A. Bruno, S. Shukla, A. Priyadarshi, N. Mathews, S. Mhaisalkar, *Energy Technol.* **2017**, *5*, 1880.

[91] B. W. Park, N. Kedem, M. Kulbak, D. Y. Lee, W. S. Yang, N. J. Jeon, J. Seo, G. Kim, K. J. Kim, T. J. Shin, G. Hodes, D. Cahen, S. I. Seok, *Nat. Commun.* **2018**, *9*, 3301.

[92] M. U. Rothmann, W. Li, J. Etheridge, Y.-B. Cheng, *Adv. Energy Mater.* **2017**, *7*, 1700912.

[93] S. Bai, Z. Yuan, F. Gao, *J. Mater. Chem. C* **2016**, *4*, 3898.

[94] S. Mabrouk, B. Bahrami, H. Elbohy, K. M. Reza, A. Gurung, M. Liang, F. Wu, M. Wang, S. Yang, Q. Qiao, *InfoMat* **2020**, *2*, 928.

[95] F. Liu, Y. Zhang, C. Ding, S. Kobayashi, T. Izuishi, N. Nakazawa, T. Toyoda, T. Ohta, S. Hayase, T. Minemoto, K. Yoshino, S. Dai, Q. Shen, *ACS Nano* **2017**, *11*, 10373.

[96] R. An, F. Zhang, X. Zou, Y. Tang, M. Liang, I. Oshchapovskyy, Y. Liu, A. Honarfar, Y. Zhong, C. Li, *ACS Appl. Mater. Interfaces* **2018**, *10*, 39222.

[97] N. Li, Z. Zhu, J. Li, A. K. Y. Jen, L. Wang, *Adv. Energy Mater.* **2018**, *8*, 1800525.

[98] J.-K. Sun, S. Huang, X.-Z. Liu, Q. Xu, Q.-H. Zhang, W.-J. Jiang, D.-J. Xue, J.-C. Xu, J.-Y. Ma, J. Ding, Q.-Q. Ge, L. Gu, X.-H. Fang, H.-Z. Zhong, J.-S. Hu, L.-J. Wan, *J. Am. Chem. Soc.* **2018**, *140*, 11705.

[99] M. Liao, B. Shan, M. Li, *J. Phys. Chem. Lett.* **2019**, *10*, 1217.

[100] J. De Roo, M. Ibáñez, P. Geiregat, G. Nedelcu, W. Walravens, J. Maes, J. C. Martins, I. Van Driessche, M. V. Kovalenko, Z. Hens, *ACS Nano* **2016**, *10*, 2071.

[101] J. Li, L. Xu, T. Wang, J. Song, J. Xue, Y. Dong, B. Cai, Q. Shan, B. Han, H. Zeng, *Adv. Mater.* **2017**, *29*, 1603885.

[102] C. Liu, Q. Zeng, Y. Zhao, Y. Yu, M. Yang, H. Gao, H. Wei, B. Yang, *Sol. RRL* **2020**, *4*, 2000102.

[103] Q. Zeng, X. Zhang, C. Liu, T. Feng, Z. Chen, W. Zhang, W. Zheng, H. Zhang, B. Yang, *Sol. RRL* **2019**, *3*, 1800239.

[104] G. R. Yettapu, D. Talukdar, S. Sarkar, A. Swarnkar, A. Nag, P. Ghosh, P. Mandal, *Nano Lett.* **2016**, *16*, 4838.

[105] J. Xue, R. Wang, L. Chen, S. Nuryyeva, T. H. Han, T. Huang, S. Tan, J. Zhu, M. Wang, Z. K. Wang, C. Zhang, J. W. Lee, Y. Yang, *Adv. Mater.* **2019**, *31*, 1900111.

[106] L. M. Wheeler, E. M. Sanehira, A. R. Marshall, P. Schulz, M. Suri, N. C. Anderson, J. A. Christians, D. Nordlund, D. Sokaras, T. Kroll, S. P. Harvey, J. J. Berry, L. Y. Lin, J. M. Luther, *J. Am. Chem. Soc.* **2018**, *140*, 10504.

[107] J. Kim, B. Koo, W. H. Kim, J. Choi, C. Choi, S. J. Lim, J.-S. Lee, D.-H. Kim, M. J. Ko, Y. Kim, *Nano Energy* **2019**, *66*, 104130.

[108] K. Chen, Q. Zhong, W. Chen, B. Sang, Y. Wang, T. Yang, Y. Liu, Y. Zhang, H. Zhang, *Adv. Funct. Mater.* **2019**, *29*, 1900991.

[109] D. Zhang, Q. Ma, H. Fan, H. Yang, S. Liu, *Carbon* **2014**, *71*, 120.

[110] B. D. Ossonon, D. Bélanger, *Carbon* **2017**, *111*, 83.

[111] Q. Wang, Z. Jin, D. Chen, D. Bai, H. Bian, J. Sun, G. Zhu, G. Wang, S. F. Liu, *Adv. Energy Mater.* **2018**, *8*, 1800007.

[112] Y. Wu, X. Yang, W. Chen, Y. Yue, M. Cai, F. Xie, E. Bi, A. Islam, L. Han, *Nat. Energy* **2016**, *1*, 16148.

[113] K. Chen, W. Jin, Y. Zhang, T. Yang, P. Reiss, Q. Zhong, U. Bach, Q. Li, Y. Wang, H. Zhang, Q. Bao, Y. Liu, *J. Am. Chem. Soc.* **2020**, *142*, 3775.

[114] X. Li, Y. Wu, S. Zhang, B. Cai, Y. Gu, J. Song, H. Zeng, *Adv. Funct. Mater.* **2016**, *26*, 2435.

[115] J. Song, J. Li, L. Xu, J. Li, F. Zhang, B. Han, Q. Shan, H. Zeng, *Adv. Mater.* **2018**, *30*, 1800764.

[116] Q. A. Akkerman, G. Gandini, F. Di Stasio, P. Rastogi, F. Palazon, G. Bertoni, J. M. Ball, M. Prato, A. Petrozza, L. Manna, *Nat. Energy* **2017**, *2*, 16194.

[117] A. Dutta, S. K. Dutta, S. Das Adhikari, N. Pradhan, *Angew. Chem., Int. Ed.* **2018**, *57*, 9083.

[118] J. B. Hoffman, A. L. Schleper, P. V. Kamat, *J. Am. Chem. Soc.* **2016**, *138*, 8603.

[119] H. Huang, Y. Li, Y. Tong, E. P. Yao, M. W. Feil, A. F. Richter, M. Doblinger, A. L. Rogach, J. Feldmann, L. Polavarapu, *Angew. Chem., Int. Ed.* **2019**, *58*, 16558.

[120] J. Dai, J. Xi, L. Li, J. Zhao, Y. Shi, W. Zhang, C. Ran, B. Jiao, X. Hou, X. Duan, Z. Wu, *Angew. Chem., Int. Ed.* **2018**, *57*, 5754.

[121] H. Yu, H. Wang, J. Zhang, J. Lu, Z. Yuan, W. Xu, L. Hultman, A. A. Bakulin, R. H. Friend, J. Wang, X.-K. Liu, F. Gao, *Small* **2019**, *15*, 1804947.

[122] J. Xi, C. Piao, J. Byeon, J. Yoon, Z. Wu, M. Choi, *Adv. Energy Mater.* **2019**, *9*, 1901787.

[123] X. Li, F. Zhang, H. He, J. J. Berry, K. Zhu, T. Xu, *Nature* **2020**, *578*, 555.

[124] W. Zhu, W. Ma, Y. Su, Z. Chen, X. Chen, Y. Ma, L. Bai, W. Xiao, T. Liu, H. Zhu, X. Liu, H. Liu, X. Liu, Y. Yang, *Light: Sci. Appl.* **2020**, *9*, 112.

[125] G. Na, L. Zhang, *Light: Sci. Appl.* **2020**, *9*, 106.

[126] F. Liu, C. Ding, Y. Zhang, T. Kamisaka, Q. Zhao, J. M. Luther, T. Toyoda, S. Hayase, T. Minemoto, K. Yoshino, *Chem. Mater.* **2019**, *31*, 798.

[127] Q. A. Akkerman, D. Meggiolaro, Z. Dang, F. De Angelis, L. Manna, *ACS Energy Lett.* **2017**, *2*, 2183.

[128] Z. Xiao, Z. Song, Y. Yan, *Adv. Mater.* **2019**, *31*, 1803792.

[129] F.-P. Zhu, Z.-J. Yong, B.-M. Liu, Y.-M. Chen, Y. Zhou, J.-P. Ma, H.-T. Sun, Y.-Z. Fang, *Opt. Express* **2017**, *25*, 33283.

[130] S. Bera, D. Ghosh, A. Dutta, S. Bhattacharyya, S. Chakraborty, N. Pradhan, *ACS Energy Lett.* **2019**, *4*, 1364.

[131] J. Shi, F. Li, J. Yuan, X. Ling, S. Zhou, Y. Qian, W. Ma, *J. Mater. Chem. A* **2019**, *7*, 20936.

[132] W. Ke, C. C. Stoumpos, M. G. Kanatzidis, *Adv. Mater.* **2019**, *31*, 1803230.

[133] L.-J. Chen, C.-R. Lee, Y.-J. Chuang, Z.-H. Wu, C. Chen, *J. Phys. Chem. Lett.* **2016**, *7*, 5028.

[134] X. Shen, Y. Zhang, S. V. Kershaw, T. Li, C. Wang, X. Zhang, W. Wang, D. Li, Y. Wang, M. Lu, L. Zhang, C. Sun, D. Zhao, G. Qin, X. Bai, W. W. Yu, A. L. Rogach, *Nano Lett.* **2019**, *19*, 1552.

[135] M. Lu, X. Zhang, Y. Zhang, J. Guo, X. Shen, W. W. Yu, A. L. Rogach, *Adv. Mater.* **2018**, *30*, 1804691.

[136] C. M. Guvenc, Y. Yalcinkaya, S. Ozen, H. Sahin, M. M. Demir, *J. Phys. Chem. C* **2019**, *123*, 24865.

[137] Z. Li, M. Yang, J.-S. Park, S.-H. Wei, J. J. Berry, K. Zhu, *Chem. Mater.* **2016**, *28*, 284.

[138] F. Li, S. Zhou, J. Yuan, C. Qin, Y. Yang, J. Shi, X. Ling, Y. Li, W. Ma, *ACS Energy Lett.* **2019**, *4*, 2571.

[139] W. Travis, E. Glover, H. Bronstein, D. Scanlon, R. Palgrave, *Chem. Sci.* **2016**, *7*, 4548.

[140] A. Dutta, N. Pradhan, *ACS Energy Lett.* **2019**, *4*, 709.

[141] F. Liu, C. Ding, Y. Zhang, T. S. Ripolles, T. Kamisaka, T. Toyoda, S. Hayase, T. Minemoto, K. Yoshino, S. Dai, M. Yanagida, H. Noguchi, Q. Shen, *J. Am. Chem. Soc.* **2017**, *139*, 16708.

[142] F. Krieg, S. T. Ochsenbein, S. Yakunin, S. ten Brinck, P. Aellen, A. Süess, B. Clerc, D. Guggisberg, O. Nazarenko, Y. Shynkarenko, S. Kumar, C.-J. Shih, I. Infante, M. V. Kovalenko, *ACS Energy Lett.* **2018**, *3*, 641.

[143] G. Li, J. Huang, H. Zhu, Y. Li, J.-X. Tang, Y. Jiang, *Chem. Mater.* **2018**, *30*, 6099.

[144] J. Pan, Y. Shang, J. Yin, M. De Bastiani, W. Peng, I. Dursun, L. Sinatra, A. M. El-Zohry, M. N. Hedhili, A. H. Emwas, O. F. Mohammed, Z. Ning, O. M. Bakr, *J. Am. Chem. Soc.* **2018**, *140*, 562.

[145] H. Bian, D. Bai, Z. Jin, K. Wang, L. Liang, H. Wang, J. Zhang, Q. Wang, S. Liu, *Joule* **2018**, *2*, 1500.

[146] Z. Huang, A. H. Proppe, H. Tan, M. I. Saidaminov, F. Tan, A. Mei, C.-S. Tan, M. Wei, Y. Hou, H. Han, S. O. Kelley, E. H. Sargent, *ACS Energy Lett.* **2019**, *4*, 1521.

[147] L. Shi, M. P. Bucknall, T. L. Young, M. Zhang, L. Hu, J. Bing, D. S. Lee, J. Kim, T. Wu, N. Takamure, D. R. McKenzie, S. Huang, M. A. Green, A. W. Y. Ho-Baillie, *Science* **2020**, *368*, eaba2412.

[148] Y. C. Zhao, W. K. Zhou, X. Zhou, K. H. Liu, D. P. Yu, Q. Zhao, *Light: Sci. Appl.* **2017**, *6*, e16243.

[149] J. S. Yun, J. Seidel, J. Kim, A. M. Soufiani, S. Huang, J. Lau, N. J. Jeon, S. I. Seok, M. A. Green, A. Ho-Baillie, *Adv. Energy Mater.* **2016**, *6*, 1600330.

[150] P. Vashishtha, J. E. Halpert, *Chem. Mater.* **2017**, *29*, 5965.

[151] C.-X. Zhang, T. Shen, D. Guo, L.-M. Tang, K. Yang, H.-X. Deng, *InfoMat* **2020**, 10.1002/inf2.12104.

[152] T. Zhang, C. Hu, S. Yang, *Small Methods* **2020**, *4*, 1900552.

[153] Y. Yuan, J. Huang, *Acc. Chem. Res.* **2016**, *49*, 286.

[154] Y. Shao, Y. Fang, T. Li, Q. Wang, Q. Dong, Y. Deng, Y. Yuan, H. Wei, M. Wang, A. Gruverman, J. Shield, J. Huang, *Energy Environ. Sci.* **2016**, *9*, 1752.

[155] D. Yang, X. Li, Y. Wu, C. Wei, Z. Qin, C. Zhang, Z. Sun, Y. Li, Y. Wang, H. Zeng, *Adv. Opt. Mater.* **2019**, *7*, 1900276.

[156] A. F. Gualdron-Reyes, S. J. Yoon, E. M. Barea, S. Agouram, V. Munoz-Sanjose, A. M. Melendez, M. E. Nino-Gomez, I. Mora-Sero, *ACS Energy Lett.* **2019**, *4*, 54.

[157] G. Li, F. W. Rivarola, N. J. Davis, S. Bai, T. C. Jellicoe, F. de la Pena, S. Hou, C. Ducati, F. Gao, R. H. Friend, N. C. Greenham, Z. K. Tan, *Adv. Mater.* **2016**, *28*, 3528.

[158] X. Zheng, S. Yuan, J. Liu, J. Yie, F. Yuan, W.-S. Shen, K. Yao, M. Wei, C. Zhou, K. Song, B.-B. Zhang, Y. Lin, M. N. Hedhili, N. Wehbe, Y. Han, H.-T. Sun, Z.-H. Lu, T. D. Anthopoulos, O. F. Mohammed, E. H. Sargent, L.-S. Liao, O. M. Bakr, *ACS Energy Lett.* **2020**, *5*, 793.

[159] Y. Wu, X. Li, H. Zeng, *ACS Energy Lett.* **2019**, *4*, 673.

[160] J. N. Yang, Y. Song, J. S. Yao, K. H. Wang, J. J. Wang, B. S. Zhu, M. M. Yao, S. U. Rahman, Y. F. Lan, F. J. Fan, H. B. Yao, *J. Am. Chem. Soc.* **2020**, *142*, 2956.

[161] M. E. Madjet, G. R. Berdiyorov, F. El-Mellouhi, F. H. Alharbi, A. V. Akimov, S. Kais, *J. Phys. Chem. Lett.* **2017**, *8*, 4439.

[162] D. Ghosh, M. Y. Ali, D. K. Chaudhary, S. Bhattacharyya, *Sol. Energy Mater. Sol. Cells* **2018**, *185*, 28.

[163] Z. Zolfaghari, E. Hassanabadi, D. Pitarch-Tena, S. J. Yoon, Z. Shariatinia, J. van de Lagemaat, J. M. Luther, I. Mora-Seró, *ACS Energy Lett.* **2019**, *4*, 251.

[164] K. Ji, J. Yuan, F. Li, Y. Shi, X. Ling, X. Zhang, Y. Zhang, H. Lu, J. Yuan, W. Ma, *J. Mater. Chem. A* **2020**, *8*, 8104.

[165] S. Christodoulou, F. Di Stasio, S. Pradhan, A. Stavrinadis, G. Konstantatos, *J. Phys. Chem. C* **2018**, *122*, 7621.

[166] S. Panigrahi, S. Jana, T. Calmeiro, D. Nunes, R. Martins, E. Fortunato, *ACS Nano* **2017**, *11*, 10214.

[167] J. B. Hoffman, G. Zaiats, I. Wappes, P. V. Kamat, *Chem. Mater.* **2017**, *29*, 9767.

[168] X. Zhang, Z. Jin, J. Zhang, D. Bai, H. Bian, K. Wang, J. Sun, Q. Wang, S. F. Liu, *ACS Appl. Mater. Interfaces* **2018**, *10*, 7145.

[169] L. Zhang, T. Hu, J. Li, L. Zhang, H. Li, Z. Lu, G. Wang, *Front. Mater.* **2020**, *6*, 330.

[170] Y. Wang, J. Tu, T. Li, C. Tao, X. Deng, Z. Li, *J. Mater. Chem. A* **2019**, *7*, 7683.

Chongming Liu is now a Ph.D. student at the State Key Lab of Supramolecular Structure and Materials under the supervision of Prof. Bai Yang, majoring in polymer chemistry and physics. He is interested in perovskite solar cells and perovskite nanocrystal-related fields including synthesis and their optoelectronic applications.

Qingsen Zeng is now a Postdoctoral Fellow at the State Key Lab of Supramolecular Structure and Materials, Jilin University. He received his Ph.D. in polymer physics and chemistry in 2019 under the supervision of Prof. Bai Yang. He is interested in polymer/nanocrystal hybrid photoelectronic materials, and now focuses on exploring new procedure to synthesize stable perovskites nanocrystals and optimizing their performance in optoelectronic devices and photocatalytic field.

Bai Yang is currently a professor of chemistry at the State Key Lab of Supramolecular Structure and Materials in the College of Chemistry, Jilin University. He received his Ph.D. in polymer physics and chemistry in 1991 under the supervision of Prof. Jiacong Shen at Jilin University. His current research interests include carbon-based nanodots (carbonized polymer dots and graphene quantum dots), polymer/nanocrystals based high-performance optical and photoelectric materials, and multiscale ordered polymeric microstructures for photonic responsive materials.